Showcasing research from Dr. Subrata Kundu's laboratory, CSIR-Central Electrochemical Research Institute (CECRI), Karaikudi, Tamil Nadu, India.

Recent advances in non-precious metal catalysts for anion exchange membrane water electrolysis

This review highlights the development of AEMWE catalyst materials with the knowledge of pilot scale single-stack electrolyzer. The current challenges and their future perspectives are discussed for scaling from pilot to industrial deployment.

Image reproduced by permission of Subrata Kundu *et al.* from *Dalton Trans.*, 2026, **55**, 540.

As featured in:

See Subrata Kundu *et al.*, *Dalton Trans.*, 2026, **55**, 540.

ROYAL SOCIETY OF CHEMISTRY

rsc.li/dalton

Registered charity number: 207890

Dalton Transactions

ROYAL SOCIETY OF CHEMISTRY

PERSPECTIVE

View Article Online
View Journal | View Issue

Cite this: *Dalton Trans.*, 2026, **55**, 540

Recent advances in non-precious metal catalysts for anion exchange membrane water electrolysis

Suprobhat Singha Roy, [a,b] Sreenivasan Nagappan, [a,b] Prasita Mazumder, [a,b] Fajar Dhanish C P, [c] Vishesh Vishesh[c] and Subrata Kundu *[a,b]

Received 23rd October 2025,
Accepted 12th December 2025

DOI: 10.1039/d5dt02543e

rsc.li/dalton

The increasing global demand for green and sustainable energy has positioned hydrogen as a crucial energy carrier. Among various production methods, water electrolysis, particularly anion exchange membrane water electrolysis (AEMWE), holds a promising technology to produce a large quantity of green hydrogen. To ensure economic viability and sustainability, it is essential to develop highly active, stable, and cost-effective non-precious metal-based electrocatalysts for AEMWE. Significant research efforts have focused on catalyst development and the overall performance of AEMWE cells in recent years, underscoring the need for a consolidated and up-to-date analysis of the field. This review provides a comprehensive overview of AEMWE technology, including its working principles, cell configurations, operational parameters, and mechanism. Furthermore, it discusses the various components of AEMWE and their impact on sustainable operation. A particular emphasis is given to a detailed survey of the recent advancements in non-precious metal catalysts for AEMWE applications. Finally, the major challenges are critically analyzed, alongside potential strategies to overcome them. Overall, this review aims to provide perspectives into current developments and outline future research directions toward achieving efficient, scalable, and sustainable hydrogen production through AEMWE.

1. Introduction

Hydrogen energy is of growing significance in the transition toward a sustainable energy future and a zero-emission economy, owing to its high gravimetric energy density of 142 MJ kg^{-1}.[1,2] Hydrogen is regarded as a promising energy carrier, holding the potential to reshape the global energy

[a]*Academy of Scientific and Innovative Research (AcSIR), Ghaziabad-201002, India. E-mail: skundu@cecri.res.in, kundu.subrata@gmail.com*
[b]*Electrochemical Process Engineering (EPE) Division, CSIR-Central Electrochemical Research Institute (CECRI), Karaikudi-630003, Tamil Nadu, India*
[c]*Centre for Education (CFE), CSIR-Central Electrochemical Research Institute (CECRI), Karaikudi-630003, Tamil Nadu, India*

Suprobhat Singha Roy

Suprobhat Singha Roy is currently pursuing his doctoral research in Dr Subrata Kundu's research group at CSIR-CECRI. He received his B.Sc. degree (2016–2019) from Ramakrishna Mission Vivekananda Centenary College under West Bengal State University, and his M.Sc. degree (2019–2021) from the School of Chemistry, University of Hyderabad. He qualified with the Joint CSIR-UGC NET examination in 2022 and has been awarded the UGC–Junior Research Fellowship. His research work mainly focuses on the development of advanced nanomaterial-based catalysts for electrocatalytic water-splitting applications.

Sreenivasan Nagappan

Sreenivasan Nagappan received his Bachelor of Science degree from Gobi Arts and Science College under Bharathiar University (2015–2018) and received his Master of Science degree from Madras University (2018–2020) with a specialization in inorganic chemistry. As he was top of the university in the M.Sc., he received a gold medal and was awarded an INSPIRE scholarship (JRF) in March 2021 by DST, New Delhi. Currently, he has been pursuing his PhD under Dr Subrata Kundu since August 2021 in the field of "Electrospun Transition Metal-based Modified Nanofibers for Water Electrolysis".

landscape and mitigate environmental challenges. Currently, conventional hydrogen production methods, such as steam methane reforming, are still dominant but are accompanied by large amounts of CO_2 emissions. While the concept of "blue" hydrogen, incorporating carbon capture and storage, has been suggested as an interim solution, the long-term vision is shifting towards "green" hydrogen produced from water electrolysis powered by renewable energy sources.[3]

Among the low-temperature water electrolysis technologies, alkaline water electrolysis (AWE) and proton exchange membrane water electrolysis (PEMWE) are the most established.[4] AWE is a relatively low-cost and has simple cell architecture, but its lower efficiency and corrosive nature in highly alkaline conditions are limiting its progress. In contrast, PEMWE enables high current densities, a compact system design, and high-purity hydrogen (>99.9%). However, its acidic environment restricts the catalyst choices to noble metals (Pt, Ir, Ru, *etc.*), significantly increasing the capital cost.[5] To overcome these limitations, AEMWE has recently emerged as a promising hybrid strategy that combines the structural and functional advantages of PEMWE with the inexpensive alkaline chemistry of AWE. Operating under mildly alkaline conditions enables AEMWE to utilize transition metal-based non-precious catalysts (Ni, Fe, Co, Mn, Cu *etc.*), thereby widening material options and reducing overall cost.[6–9] Additionally, the broad compositional tolerance in the alkaline environment offers a versatile platform for advanced catalyst design by alloying, heteroatom doping, and defect engineering to maximize electronic structure, boost active site accessibility, and enhance catalytic turnover.

Over the past decades, numerous transition metal-based catalysts have been developed, demonstrating high efficiency for oxygen evolution reaction (OER) and hydrogen evolution reaction (HER) processes in alkaline conditions.[10–12] Having overall good water-splitting performances, many researchers employed these catalysts in a stack cell AEMWE device. NiFe-based catalysts have consistently shown superior OER activity, while NiMo-based catalysts are recognized as the most effective for HER in AEMWE systems, although other variations and compositions of metal ions with significant performance are also being reported.[13] A few review articles recently have summarized the development of OER and HER catalysts for AEMWE.[14,15] However, the relevant discussions regarding AEMWE operations and catalyst development are relatively limited in scope. Considering future possibilities of the AEMWE technology, it is required to understand the rationale of catalyst development and the current progress of catalyst development in this field. Also, the transition from lab scale OER/HER study to AEMWE study is required to evaluate their performance at a pilot scale. Apart from that, the stack cell parameters, such as membrane electrode assembly (MEA) fabrication method, temperature, analyte flow design, *etc.*, also need to be analyzed to achieve a high-performance technology.

In this review we have comprehensively summarized various water electrolysis technologies and emphasized the significance of AEMWE for the next-generation technology for green hydrogen production. The composition and operating mechanisms of the AEMWE device are systematically discussed, with particular attention to strategies for improving performance and durability. A major focus is given to non-precious metal-based catalyst development and their design strategies. The performance benchmark at the pilot scale with these materials was also highlighted. Furthermore, we have provided current challenges in the pilot scale of water electrolysis and their possible solutions to make a significant jump to the industrial scale. This review will help the reader to understand the AEMWE components, their optimum utilization, catalyst development, their performance status, challenges, and future opportunities for the next-generation green hydrogen production technology.

Prasita Mazumder

Prasita Mazumder received her Bachelor of Science degree from Jadavpur University (2018–2021) and received her Master of Science degree from Jadavpur University (2021–2023) with a specialization in inorganic chemistry. She was awarded an INSPIRE scholarship (JRF) in February 2024 by DST, New Delhi. Currently, she has been pursuing her PhD under Dr Subrata Kundu since August 2024 in the field of "Functionalized Metal–Organic Frameworks as Noble Metal-Free Electrocatalysts for Water-Splitting Application".

Fajar Dhanish C P

Fajar Dhanish C P is currently pursuing his Bachelor of Technology (B.Tech.) in Chemical and Electrochemical Engineering at the CSIR-Central Electrochemical Research Institute (CECRI), Karaikudi, Tamil Nadu, India, affiliated with Anna University (2022–2026), Chennai. He is presently working as an undergraduate research student under the guidance of Dr Subrata Kundu, focusing on the design and development of advanced electrocatalysts for water-splitting applications.

2. Modern technologies for water electrolysis

AWE is easy to operate among the available electrolysis systems and is currently being used at the megawatt scale with two electrodes submerged in highly concentrated aqueous alkaline electrolytes (KOH or NaOH).[16] A traditional AWE system uses nickel or steel electrodes separated by a porous diaphragm. Although conventional AWE has considerable advantages, it also has serious limitations, such as operating with corrosive electrolytes, limited mobility of hydroxide ions, efficiency losses (inefficiencies), and hydrogen–oxygen mixing, which makes it difficult to adapt to intermittent renewable energy sources. In response to these limitations, PEMWE technology was introduced in the 1960s, marking a significant breakthrough in the hydrogen industry.[16] In PEMWE systems, the liquid alkaline electrolyte is replaced with a solid proton-conducting polymer membrane, which simultaneously transports protons and acts as a gas separator for the anode and cathode. This setup allows high current densities (≈2 A cm^{-2}) under moderate temperatures (50–80 °C), where the use of platinum group metal catalysts (Pt for cathode and IrO_2 for anode) facilitates exceptionally fast HER kinetics.[17] However, the corresponding acidic environment requires highly corrosion-resistant parts, including catalysts, current collectors, and bipolar plates. Consequently, rare and expensive materials (Ir- and Pt-based catalysts, Ti-based components, *etc.*) are needed. These materials are particularly scarce (≈0.001 ppm in the Earth's crust) and, therefore, have limited annual production. The rising demand for these limited materials in other industries also puts upward pressure on the price of these materials, which directly translates into high capital costs of PEM electrolyzers, which are estimated at USD 1100–1800 per kWe in the International Renewable Energy Agency (IRENA) report.[19] Although PEMWE offers compact, efficient, and high-rate hydrogen production compared to AWE, it relies on rare materials, which pose a significant obstacle to scaling up. These limitations have driven research into AEMWE, which combines the advantages of both PEMWE and AWE. Like PEMWE, AEMWE uses a solid polymer electrolyte, which separates the anode and cathode compartments, but it is an alkaline rather than acidic operation. The foremost rationale for the development of AEMWE is to diminish the cost since Earth-abundant, non-precious metal catalysts such as nickel, cobalt, *etc.* can be used.[13] A general comparison table of these technologies is represented in Table 1.[18] AEMWE devices can use either pure water or low concentrations of alkaline feed, such as dilute KOH solutions. While it is currently at a lab scale, it is still an emerging low-temperature electrolysis technology that has several advantages, including low cost. One distinct feature of AEMWE is its zero-gap cell design, which reduces gas crossover, hence improving the purity of both hydrogen and oxygen gas and increasing the energy efficiency. Lower cell resistance enhances the overall performance of AEMWE by enabling higher current densities. This improvement allows for more compact system designs, reduced catalyst mass loading, and a smaller overall stack footprint. Despite these advantages, several challenges persist for AEMWE, including the limited stability of OER catalysts, low ionic conductivity of anion exchange membranes, and issues related to MEA construction and long-term durability. To guide its development, the IRENA has set an ambitious target for AEMWE technology by 2050:

Vishesh Vishesh

Vishesh Vishesh is currently pursuing a B.Tech. in Electrochemical and Chemical Engineering at CSIR-Central Electrochemical Research Institute (CECRI), Karaikudi, India. He is working under the guidance of Dr Subrata Kundu, and his research focuses on the green synthesis, characterization, and electrochemical evaluation of nanomaterials for diverse applications, including sustainable energy conversion, environmental remediation, catalysis, and water splitting. His work involves exploring eco-friendly synthesis routes, material optimization, and performance enhancement for next-generation electrochemical systems.

Subrata Kundu

Dr Subrata Kundu received his PhD from the Indian Institute of Technology (IIT), Kharagpur, India, in early 2005. Then he moved to the University of Nebraska, Lincoln, USA, and later to Texas A&M University, College Station, Texas, USA, as a post-doc fellow (from 2005 to 2010). He is currently working as a senior principal scientist at CSIR-CECRI, Karaikudi, India. Dr Kundu is a Fellow of the Royal Society of Chemistry (FRSC) and has been serving as an associate editor of the prestigious 'Journal of Materials Chemistry A' and 'Materials Advances' from RSC publishers since 2022 and 'Scientific Reports' from Nature Group Publishers since 2015. He has recently been appointed as an Editorial Advisory Board member of the prestigious 'ACS Applied Materials & Interfaces'. Dr Kundu and his co-workers are working in the forefront area of materials sciences with an emphasis on energy, environment, catalysis, and electrocatalysis applications.

Table 1 Characteristics' comparison of AWE, PEMWE, and AEMWE technologies.[18] (Here, SS = stainless steel; NF = Nickel foam; CC = Carbon cloth; GDL = Gas diffusion layer)

Parameters	AWE	PEMWE	AEMWE
Operating temperature (°C)	70–90	50–90	25–80
Operating pressure (bar)	1–30	<70	<35
Electrolyte (mol L^{-1})	KOH (5–7)	Pure water	Pure water or KOH (0.1–1)
Separator	Diaphragm	PEM	AEM
Anode catalyst	Ni-based oxides or alloys	IrO_2/RuO_2	NiFe or NiFeCo alloys/oxyhydroxides
Cathode catalyst	Ni-coated SS or alloys	Pt/C	NiMo alloys
Anode GDL	Not always present	Ti mesh	NF
Cathode GDL	Not always present	Ti mesh	NF or CC
Bipolar plates	Not always present	Ti or Pt-coated Ti	SS or Ni-coated SS
Current density/voltage range	0.2–0.8 A cm^{-2}/1.4–3.0 V	1.0–2.0 A cm^{-2}/1.4–2.5 V	0.2–2.0 A cm^{-2}/1.4–2.0 V

achieving current density >2 A cm^{-2} at <2 V with operational durability of up to 100 000 hours.[19] However, current AEMWE systems typically operate at lower current densities with limited long-term durability. Therefore, to tackle these challenges and meet the target, it is important to understand the AEMWE mechanism and to develop its components, especially catalyst materials and membranes.

3. Overview of components and mechanism of AEMWE devices

The majority of the materials and components currently used in AEMWE devices have been adapted from AWE and/or PEMWE. Hence, there exists substantial scope for continued research and innovation. In contrast to PEMWE, where components and assembly protocols have been standardized or benchmarked internationally, AEMWE lacks a universally accepted configuration or performance standard.[20–22] The general architecture of zero-gap AEMWE devices for single-cell stack cells is discussed briefly below with a note that commercial multi-stack electrolyzers may have different design considerations, which are beyond the scope of this review.[23–25] A typical AEMWE cell comprises several key components: an MEA, gaskets, bipolar plates (BPP) with flow field, current collectors, and end plates, as illustrated schematically in Fig. 1a.

3.1. Membrane electrode assembly (MEA)

The MEA is the core of the AEMWE device and is a sandwich structure consisting of an AEM with catalyst layers (CLs) and a GDL or porous transport layer (PTL) on each side. The MEA represents the complete assembly that is present between the bipolar plates, serving as the functional heart of the electrolyzer. Typically, it has a symmetrical configuration at the center, layered as GDL/CL/AEM/CL/GDL (Fig. 1a). All these components need to be fully functional in order to have efficient water electrolysis. The physical and electrochemical properties of each MEA component are summarized in Fig. 1b, highlighting their role in AEMWE.

The AEM is one of the most important components of the AEMWE electrolyzer. The typical function of the AEM is to transport the hydroxide ions across the membrane. Also, it acts as a separator of gaseous hydrogen and oxygen products, produced during the reaction. It is typically composed of a long-stranded polymer backbone (generally polysulfone or polystyrene cross-linked with divinylbenzene) with anion exchange functional groups such as quaternary ammonium salts, $-NH_3^+$, $-RNH_2^+$, $-R_3P^+$, $-R_2S^+$ *etc*. A detailed discussion on different AEMs and their performances can be found in previously reported articles.[26–29] In general, an ideal AEM should exhibit high ionic (hydroxide ion) conductivity, excellent thermal, mechanical, and chemical stability, and low specific resistance to ensure efficient and durable operation of the AEMWE system.[29]

There are two widely adopted methods generally used to prepare the MEA. In one method, the CLs are coated directly on each side of the membrane followed by the assembly of GDLs, known as the catalyst-coated membrane (CCM) method. Alternatively, the CLs are coated over the conductive substrate (*e.g.* GDL)[30] followed by sandwiching using the AEM, known as catalyst-coated substrate (CCS) method.[31] To prepare a CCM or CCS, a catalyst ink is generally prepared that is composed of water, alcohol, and a binder or ionomer. An optimized ratio of ionomer and catalyst is highly desired for reducing the mass/ion transport resistance and for good adhesion between ionomer, membrane, and electrode.[32–35] Typically, anion exchange ionomers are preferred to prepare the catalyst ink rather than Nafion for better ion transport in AEMWE.[36] While the CCM method is well established in PEMWE, the preferred approach for AEMWE is still under investigation. Although direct catalyst coating on AEMs possesses difficulties like swelling and shrinking, recently several studies showed promising performance by adopting the CCM method of MEA formation.[37–40] For instance, Klingenhof *et al.* applied a direct coating on AEM using the wet-film bar coating method, which was stabilized and protected using a combination of a polytetrafluoroethylene (PTFE) inner foil and an adhesive outer foil. They fabricated an NiFe-LDH (layered double hydroxide) anode catalyst layer on the AEM, which showed promising AEMWE performance by operating at a voltage below 1.8 V at a current density of 2 A cm^{-2} at 80 °C with decent stability for 110 hours.[41] Similarly, extensive studies were done on the CCS method for MEA fabrication also.[42–44] Galkina *et al.* prepared Ni_3Fe-LDH coated on a Ni PTL using

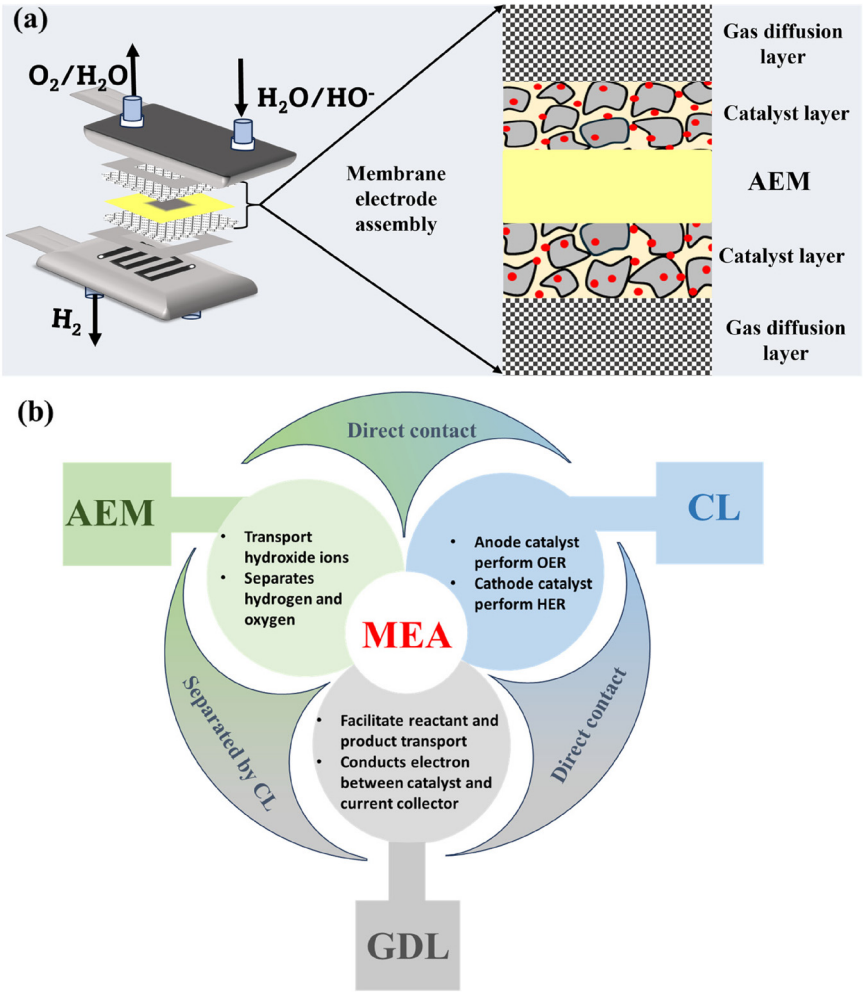

Fig. 1 (a) Typical representation of a single stack AEMWE device; (b) the overview of the components of an MEA.

the CCS method, achieving 2 A cm^{-2} at 2 V and 60 °C, and 1000 hours of stability with a degradation rate of 84 μV h^{-1}.[45] A hybrid approach combining both the CCS and CCM methods on the opposite sides of the MEA has also been reported to enhance the overall performance.[46] Although these methods were reported extensively, both the CCS and CCM methods have their own advantages and disadvantages. For example, the CCM method allows direct contact between the catalyst and membrane, which facilitates the ion transport, minimizes charge transfer resistance, and maximizes the electrochemically active surface area. However, this method requires precise coating control to prevent membrane damage and leaks, which can affect long-term durability. On the other hand, CCS methods are easy to implement and can utilize an effective and rigid GDL or PTL as a substrate, which minimizes membrane degradation and enhances mechanical durability. However, its possesses high interfacial resistance, and poor utilization of the electrochemically active surface area. Although hot-pressing the CL and AEM minimizes these drawbacks, CCM is still preferred in terms of high activity and low interfacial resistance. Often, the ionomer decreases the ion/mass transport or prevents the active material from being fully exposed to the reactant, and hence an increase in ionomer content affects the performance of the catalyst. However, the *in situ* material grown over the surface of a GDL or PTL or even on an AEM resolves the issue of the requirement for an ionomer and associated drawbacks.[48] The MEA fabrication using a self-supported electrode (SSE), where the catalyst material is grown directly on a GDL such as NF, offers a significant advantage over the CCS method, as this method is binder-free. Moreover, the direct interfacial contact between the catalyst and AEM markedly reduces interfacial resistance. The resistance could be further minimized if the catalyst material is directly grown on the membrane or *vice versa*. In a recent study, Wan *et al.* adopted a swelling-assisted transfer method to form an anode catalyst layer (ACL) on an AEM (Fig. 2a). They first synthesized a nanoarray of anode catalyst on nickel foil and subsequently deposited the ionomer to achieve a uniformly distributed AEM surface. Utilizing the swelling behaviour of the AEM in deionized water at 50 °C, they successfully detached the nickel foil, thereby forming a three-dimensional ACL/AEM structure. In parallel, they also

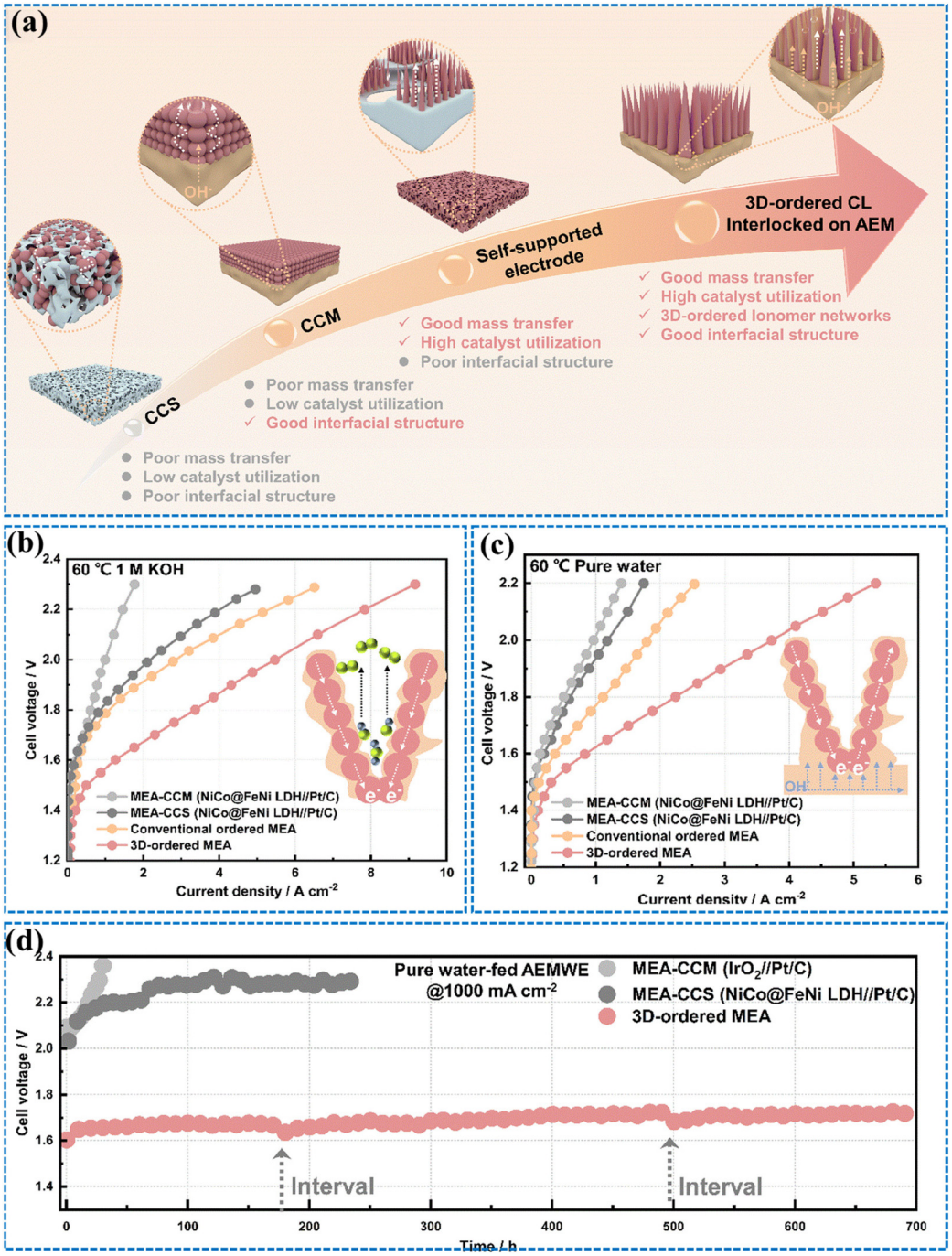

Fig. 2 (a) Design strategy for 3D-ordered ACLs in an MEA with the advantages and disadvantages of CLs prepared using different methods; AEMWE performance of different MEAs including CCM, CCS, 3D-ordered MEA prepared by a conventional decal transfer and 3D-ordered MEA prepared by a swell-assisted transfer method: (b) under ambient pressure at 60 °C for 1 M KOH solution flowing in both the anode and the cathode, and (c) under ambient pressure at 60 °C for pure water flowing in both the anode and the cathode; (d) long-term stability performance of a water-fed AEMWE device at 1000 mA cm^{-2} and 60 °C.[47] Reprinted with permission from ref. 47. Copyright 2024 Royal Society of Chemistry.

fabricated MEA with CCS, CCM, and conventional ordered methods for comparative evaluation. As shown in Fig. 2b and c, at 60 °C in 1 M KOH and pure water, the current densities followed the order: CCM < CCS < conventional ordered MEA < 3D-ordered MEA. Furthermore, they have observed that this 3D-order MEA technique has exceptional stability in 1 M KOH solution with a low voltage degradation rate of 120 μV h^{-1} at 8 A cm^{-2} current density for 1000 hours at 60 °C. In a pure water-fed condition, a voltage degradation rate of 71 μV h^{-1} at 1 A cm^{-2} current density for 700 hours was also observed (Fig. 2d).[47] These studies highlight the importance of MEA fabrication for optimized AEMWE performance.

3.2. Other components of AEMWE

At the laboratory scale, the common design of AEMWE devices is generally square-shaped, although a few studies have also reported polygonal or circular or a combined variant design.[49–51] Regardless of the geometry, gaskets are employed between the MEA and BPP to compensate for pressure non-uniformities caused by variations in the GDL thickness and to ensure a tight seal that prevents leakage. The materials for the gasket need to possess strong alkali resistance and a high fusion point (>200 °C); suitable examples include Teflon, polytetrafluoroethylene (PTFE), and perfluoroalkoxy (PFA).[25] The next component is BPP material with a flow field that facilitates electrolyte distribution within the cell. Typically, these BPPs are made of stainless steel or nickel or nickel-coated stainless steel for robust stability and corrosion resistance behavior under alkaline conditions.[25] Being electronically conductive, these plates can also function as current collectors. Alternatively, a separate current collector made of Au-plated Cu can also be used, as bare Cu is prone to corroding in alkaline conditions.[52] At either end of the cell stack, end plates are placed, which have threaded bolts that provide the compression to the cell. The end plates need to be hard, rigid, and corrosion resistant and must withstand mild temperatures (40–80 °C for AEMWE). Acrylic- or polypropylene-based end plates are favored for lab scale as they are chemically inert and insulating in nature. For excellent mechanical strength and endurance, Ni or stainless steel also can be used.[53,54]

3.3. Operating mechanism of AEMWE

In an AEMWE device, water splits into H_2 and O_2 at the cathode and anode, respectively, under pure water conditions or alkaline conditions, where HO^- serve as charge carriers. In contrast, in PEMWE, H^+ serves as the charge carrier. The fundamental operating mechanism in PEMWE is that H_2O is supplied to the anode side, where it is oxidized to O_2 (eqn (1)) and H^+, followed by transportation of H^+ through the PEM to the cathode side, where it will reduce to H_2 (eqn (2)). This mode of operating mechanism is often known as dry cathode operation, because no electrolyte is directly supplied to the cathode side.

Anode:

$$2H_2O \rightarrow O_2 + 4H^+ + 4e^- \quad (1)$$

Cathode:

$$4H^+ + 4e^- \rightarrow 2H_2 \quad (2)$$

Overall:

$$2H_2O \rightarrow 2H_2 + O_2 \quad (3)$$

This is considered to be advantageous in terms of ease of separation of H_2 and its high purity. In contrast, in AEMWE, since the charge carrier is HO^-, the basic operating mechanism is to supply the electrolyte from the cathode side. The H_2O molecules will reduce to the cathode side to generate H_2 and HO^- (eqn (4)), followed by HO^- transportation to the anode side *via* the AEM to oxidize to O_2 molecules (eqn (5)), known as dry anode operation.

Cathode:

$$4H_2O + 4e^- \rightarrow 2H_2 + 4HO^- \quad (4)$$

Anode:

$$4HO^- \rightarrow O_2 + 2H_2O + 4e^- \quad (5)$$

Overall:

$$2H_2O \rightarrow 2H_2 + O_2 \quad (6)$$

However, various operating conditions can be employed in AEMWE, including dry anode, dry cathode, and both wet conditions, and the optimal operating mechanism is yet to be exclusively benchmarked. AEMWE operating in dry anode conditions depends primarily on AEM's HO^- transport capabilities. As there is no supply of anolyte to the anode side, the overall performance of the AMEWE cell depends majorly on AEM's ion transport efficiency, *i.e.*, the ionic conductivity of the AEM. This mode is particularly suitable when pure water is used as the feed, as hydroxide ions are generated *in situ* at the cathode. Conversely, when the dry cathode mode is operational in an AEMWE cell, the use of KOH solution is preferred as HO^- is the reactant at the anode. In this case, water molecules are co-transported along with hydroxide ions from the anode to the cathode *via* electroosmotic drag, where they are subsequently reduced to produce hydrogen. The advantage of the dry cathode condition is that there is no need for further purification of H_2. On the other hand, the dry anode condition can be used when pure water is fed to the cell to avoid corrosion in high alkali conditions. As the KOH-containing electrolyte has better ionic conductivity than pure water, the voltage input and thereby energy consumption is less in the cell operating in dry cathode mode.[56] At elevated current densities, operation under one-side dry conditions may lead to a severe performance degradation during long-term studies. In particular, the cell operating in dry cathode conditions might face the problem of the membrane drying out due to fast reaction at high current densities. To validate this, Koch *et al.* investigated dry cathode operation in an AEMWE cell *via in situ* neutron imaging at various current densities (Fig. 3). Their studies confirmed that the dry cathode operation leads to an imbalanced water distribution in the MEA where the high-water content is present at the anode side with a gradient towards the cathode side. This water imbalance becomes more pronounced at higher current densities, as the water at the cathode is predominantly consumed in the reduction reaction and is simultaneously transported to the anode through electro-osmotic drag (Fig. 3a). Furthermore, the same study was conducted to compare two cathodes with varying ion exchange capacity (IEC) ionomers. The findings revealed that the cathode containing a high IEC ionomer exhibited superior water retention within the MEA across all current densities, compared to the one with a relatively low IEC ionomer. The polarization data confirmed that the high-IEC cell demanded a lower overpotential at a particular

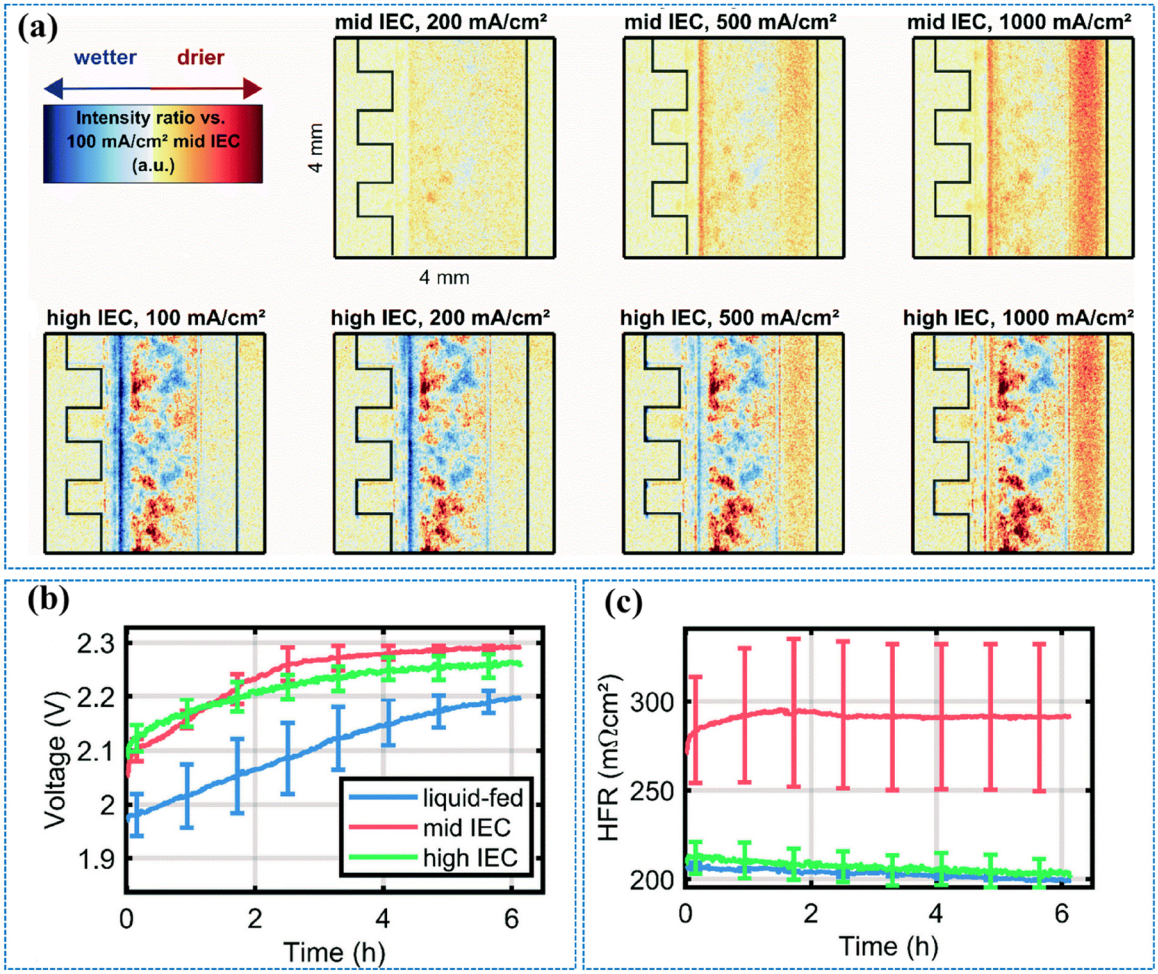

Fig. 3 Relative drying of the AEMWE device fed with 0.1 M KOH only on the anode side with (a) a mid IEC (1.8–2.2 meq. g^{-1}) cathode and a high IEC (2.3–2.6 meq. g^{-1}) cathode. White denotes no change in neutron intensity, blue an increase in water content (lower intensity) and yellow to red a decrease in water content. (b) Short-term degradation during a 1 A cm^{-2} current held over up to six hours; (c) high frequency resistance during six-hour measurement.[55] Reprinted with permission from ref. 52. Copyright 2022 Royal Society of Chemistry.

current density than the mid-IEC cell (Fig. 3b). However, when electrolyte was fed to both sides, the activity of the cell increased. Also, the stability test for 6 hours at 1 A cm^{-2} current density shows that both the wet cathode and the high-IEC dry cathode degraded with a rate of 45 mV h^{-1}, while the mid-IEC cathode degraded with a rate of 75 mV h^{-1} (Fig. 3c).[55] Hence, operating under both-side wet conditions not only mitigates membrane dehydration but also enhances catalyst activity at high current densities, contributing to improved long-term cell durability. Additionally, both-side continuous flow facilitates efficient removal of gas bubbles for better performance of the cell. Generally, the overall AEMWE performance is affected by the collective nature of its components and the chosen operating mechanism. Hence, it is essential to optimize all the components, along with the operating conditions and mechanisms, to achieve the best performance. In the literature, only cathode side,[50,57–61] only anode side,[62–68] and both side flow[69–74] of electrolyte are reported, where the researchers optimized their cells according to the working conditions.

Considering AEMWE's performance, the catalyst material plays a pivotal role in governing the electrochemical reactions, directly impacting the overall cell performance. Consequently, careful consideration of the catalyst selection and design is important. In the following section, the rationale behind the development of non-precious catalyst materials is discussed in detail, highlighting their design strategies, performance characteristics, and potential advantages for AEMWE application.

4. Recent development of non-precious catalysts for AEMWE

AEMWE relies on two key electrochemical reactions known as OER at the anode and HER at the cathode. Although platinum group metals (PGMs) exhibit good activity towards the OER/HER, their scarcity and cost are a major concern. Therefore, to enable cost-effective production of green hydrogen *via* AEMWE

technology, the development of non-precious, Earth-abundant, and effective electrocatalysts to catalyze both the OER and HER is necessary. AEMWE can utilize Earth-abundant transition metal-based catalysts as it operates in alkaline or near-alkaline conditions. Therefore, a significant effort has been made to develop highly efficient and cheap transition metal-based catalysts. In order to meet the requirement of industrial applications, high-performance electrocatalysts should satisfy the following minimum criteria: (1) they should deliver 1 A cm^{-2} current density at minimum overpotential or voltage input; (2) they must maintain their electrochemical and mechanical stability at ≥1 A cm^{-2} for a prolonged time at industrial conditions (~60 °C, pure water, 0.1 M, or 1 M KOH solution); and (3) their production should be scalable, reproducible, and economically viable.[16]

Transition metals represent a rational and strategic choice to satisfy the abovementioned criteria by catalyzing the OER/HER processes in alkaline conditions, owing to their versatile redox chemistry and unique electronic structure.[75–77] Transition metals like Ni, Co, Fe, Mo, *etc*. have unique electronic structures and favorable redox characteristics. Their partially filled d-orbitals enable fast electron transfer with multiple accessible oxidation states, which effectively modulates the binding energies with reaction intermediates for favorable reaction kinetics.[78–80] According to the Sabatier principle, reactions passing through surface-adsorbed intermediates require optimum adsorption/desorption of the intermediates for facile catalysis. If the binding energy is too strong, the intermediates accumulate at the surface and poison the active sites, whereas if the binding energy is too weak, reaction intermediates cannot be stabilized and thereby impede the catalytic process.[81] Transition metals, in particular Ni, Co, Fe, Mo, *etc*., are particularly attractive to catalyze the OER/HER process as either pure metals, alloys, oxides, hydroxides, sulfides, phosphides, or complex structures like layered hydroxides, dichalcogenides, or metal–organic frameworks (MOFs).[82–87] The advantage of utilizing these materials is that they allow tuning of their properties by several modifications such as doping, defect-site creation, heterostructure creation, interfacial engineering, and nano-structuring. Such approaches enable the optimization of catalytic performance by improving active site accessibility, conductivity, and stability. The following subsections subsequently discuss the development of these materials for AEMWE applications.

4.1. Layered double hydroxides (LDHs)

LDH materials attracted considerable attention as electrocatalysts in the past decade. Owing to their ease of synthesis, large surface area, good activity, and stability, LDHs represent an excellent choice of materials for the OER/HER in alkaline media. Among all LDH materials, NiFe-LDH is widely recognized as the most efficient for the OER in alkaline conditions.[88] These materials serve as pre-catalysts for the OER process, where highly active metal oxyhydroxides (*e.g.*, NiFeOOH) are the actual catalysts that are responsible for the OER process.[89,90] The OER activity of LDH materials is strongly influenced by the metal ratio (Ni/Fe or, in general, the M/M′ ratio), which affects their crystallinity and local electronic environment. Jiang *et al.* reported that with increasing Fe/Ni ratio, the crystallinity decreases. They have observed a higher Fe^{2+} content with increasing Fe/Ni ratio, where Fe^{2+} gradually substitutes the Ni host matrix, leading to higher structural disorder in NiOOH. Consequently, the OER activity was found to be Ni_3Fe > Ni_3Fe_2 > $NiFe_3$-LDH; *i.e.*, with increasing Fe/Ni ratio, the activity decreased. *In situ* Raman studies revealed that the more disordered Ni_3Fe_2 and $NiFe_3$ LDHs show an irreversible phase transition during the potential change, whereas the more ordered Ni_3Fe-LDHs were able to return to the initial stage with good crystallinity. Furthermore, they have employed Ni_3Fe-LDH in AMEWE as the anode material and achieved 2.07 A cm^{-2}@2 V with stable operation for 400 hours at 1 A cm^{-2} current density with a degradation rate of 0.1 mV h^{-1}.[91] Several other studies reported utilizing NiFe-LDH as an anode catalyst with high stability at 1 A cm^{-2} for 1000,[92] 9000 hours.[93] Furthermore, surface engineering *via* doping of Co, and W in NiFe-LDH also showed promising performance for AEMWE as an anode catalyst.[94–96]

Although LDH materials are promising OER catalysts for AEMWE, their performance degradation is often observed at high current densities (≥1 A cm^{-2}). This could be attributed to local pH change, excessive bubble formation, and chemical degradation, which were tackled by several researchers *via* morphology modulation, interlayer engineering, and nanostructuring methods.[97–99] One of the strategies proposed by Li *et al.*, who enhanced the transport of HO^- between the membrane and catalytic interfaces, successfully regulated the local pH change for enhanced long-term AEMWE operation. For that, they have introduced a hierarchical zwitterion-NiFe-LDH interface where the cationic moieties of the zwitterions help to transport OH^- across the electrode–membrane interface (Fig. 4a). This strategy enabled a dynamic OH^- transport network that neutralized accumulated H^+ during the OER process. Consequently, in practical AEMWE, the z-NiFe-catalyzed AEMWE device exhibited a low cell voltage of 1.76 V at 1 A cm^{-2} and long-term stability over 14 000 h, with a voltage degradation rate of 12.3 μV h^{-1} (Fig. 4b and c).[100]

In addition to pure alkaline water, seawater electrolysis gained attention due to its natural abundance. However, H_2 production *via* seawater electrolysis is challenging due to the complex composition of seawater. The presence of ions such as Cl^-, and Br^-, along with various microorganisms, promotes material corrosion and inhibits the desired catalytic process. Therefore, the catalyst must possess strong corrosion resistance and high selectivity toward H_2O or HO^-. This can be achieved by developing corrosion-resistant materials with high selectivity for the water-splitting reaction. In a recent study Saada *et al.* showed that NiFe-LDH deposited on NiCr foam showed excellent corrosion resistance during seawater electrolysis,[51] where Cr played a major role as a Cl^- repellent, consistent with the findings of a few other studies.[102,103] Enhancing mass and electron transfer, particularly through materials with strong electron-capturing capabilities, can facilitate the for-

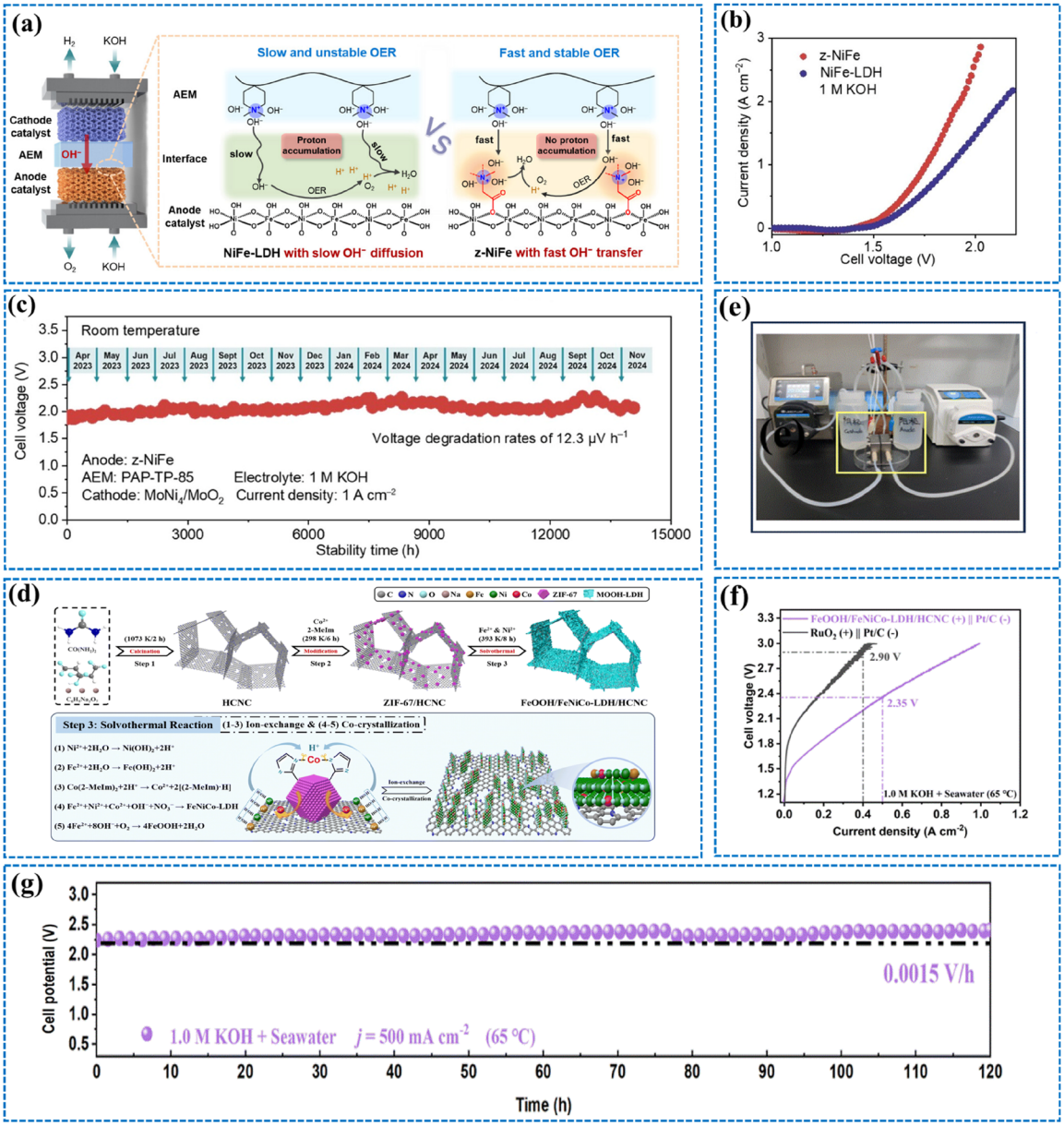

Fig. 4 (a) Schematic representation of the enhancement of HO-transfer using quaternary ammonium cations across the AEM–anode interface; (b) polarization curves of z-NiFe and NiFe-LDH as the anode measured in the 1 cm^2 AEM-WE device at 25 °C; (c) durability test of the 1 cm^2 AEM-WE device using z-NiFe//$MoNi_4/MoO_2$ at 1000 mA cm^{-2} in 1 M KOH.[100] Reprinted with permission from ref. 73. Copyright 2025 Wiley-VCH. (d) Schematic illustration for the fabrication of FeOOH/FeNiCo-LDH/HCNC; (e) digital photograph of an FeOOH/FeNiCo-LDH/HCNC-based AEM electrolyzer; (f) polarization curve and (g) stability study of FeOOH/FeNiCo-LDH/HCNC-based AEM electrolyzer measurements in alkaline seawater.[101] Reprinted with permission from ref. 74. Copyright 2025 Royal Society of Chemistry.

mation of OER active species with improved kinetics, thereby promoting efficient seawater electrolysis, as observed by Luo *et al.* in their recent study. They have used a self-sacrificing and dual-ion etching (SSDIE) strategy to develop FeOOH/FeNiCo-LDH heterogeneous nanosheets on honeycomb-channel N-doped carbon (HCNC), as shown in Fig. 4d. The strong hydrogen/electron capturing ability of FeOOH along with the rapid mass/electron transfer efficiency of conductive HCNC in FeOOH/FeNiCo-LDH/HCNC collaboratively accelerated the reconstruction process for a faster OER, leading to efficient seawater electrolysis. The electrolyzer setup is shown in Fig. 4e, and the activity and stability in seawater showed a decent performance, as shown in Fig. 4f and g.[101]

Along with NiFe-LDH, other LDHs such as NiCo-LDH, NiCoFe-LDH, and CoFe-LDH have also been explored for AEMWE applications.[104–106] However, the HER performance of bare LDHs is not as promising as noble metal Pt. Although a few reports employed the modified or surface-engineered LDHs as both cathode and anode catalyst,[50,70] many reports have used LDH as the anode and NiMo alloy as the cathode

material in AEMWE.[107,108] Recent studies showed that the presence of Mo and Ni as an alloy or as nanocomposite gives a performance similar to or often better than Pt.[109,110] Nonetheless, LDH materials are promising electrocatalysts as anode material for AMEWE applications.

4.2. Metal oxides

Among transition metals, elements such as Ni, Fe, and Co have been widely utilized in their oxide forms as catalysts for the OER/HER. Compared to monometallic oxides, bimetallic or mixed metal oxides (MMO) generally exhibit superior performance. Recent studies investigated this class of materials for AEMWE applications. Extensive works on $NiFe_2O_4$ and derivative materials were reported in the past. For instance, Wang *et al.* reported 1.66 V cell voltage and 1000 hours of stability (with minimal 0.24 mV h^{-1} voltage decay) at 1 A cm^{-2} current density using $NiFe_2O_4$ as the anode catalyst material. Furthermore, they have optimized the mass loading, and they observed that the activity trend varied with mass loading as 2.5 > 1.0 > 3.5 mg cm^{-2}. With optimized mass loading, they have observed a high current density of 4.0 A cm^{-2} at 1.89 V applied voltage.[111] In a different study, Yoon *et al.* reported Ti-doped $NiFe_2O_4$ as an anode catalyst for high-performance AEMWE application.[112] Apart from $NiFe_2O_4$, other mixed metal oxides such as $NiMn_2O_4$,[113] $NiCo_2O_4$,[114] and $Cu_{0.5}Co_{2.5}O_4$ [115] were also reported as anode catalysts for AEMWE. However, those studies used the noble metal Pt as the cathode catalyst in their AEMWE configuration. Among non-noble metals, NiMo-based material showed good performance as a cathode material towards the alkaline HER.[110] In their study Cui *et al.* demonstrated an AEMWE configuration by using $NiFeMo_4$ as a pre-catalyst for the anode material and $MoNi_4$ as the cathode material. The overall system showed 1000 hours of stability at 1 A cm^{-2} current density with a rate of voltage decay of 130 μV h^{-1}.[116] In alkaline conditions, the HER process is initiated by the cleavage of H–OH bonds, which often requires high energy input for most catalysts. However, Ni and Mo work synergistically to facilitate the process and therefore reduce the high energy input. To validate this, Lin *et al.* introduced NiMo/MoO_2 as an HER catalyst *via* an interlayer anchoring strategy (denoted as NiMo/Int/NF) to achieve high activity and stability at a high current density. The NiMo/Int/NF catalyst surpassed Pt/C in terms of activity, as demonstrated in Fig. 5a. Based on the Tafel slope (derived from the steady-state potential), the *in situ* Raman study (in a mixed solution of $KHCO_3$ and K_2CO_3), the EIS study, and the *in situ* XRD study, they have concluded that the rate-determining step (RDS) is the Volmer step for NiMo/Int/NF, whereas for Pt/C it is the Heyrovsky step (Fig. 5b). Therefore, the heterostructure benefited the fast Volmer step (RDS), thereby accelerating the overall hydrogen evolution kinetics. Moreover, the interlayer structure was shown to enhance the mechanical robustness of the catalytic layer. With the integration of NiMo/Int/NF as the cathode material and CAPist-L1 as the anode material in the AEMWE device (Fig. 5c), the cell achieved 1 A cm^{-2} current density at 1.78 V (Fig. 5d). Furthermore, the device achieved robust stability for 3000 hours at 1 A cm^{-2} with a voltage decrease rate of 22.8 μV h^{-1} (Fig. 5e).[117]

Apart from NiMo-based catalysts, NiCu-MMO was also reported as a cathode catalyst for AEMWE.[33] Other studies also have utilized different cathode materials. For example Liang *et al.* used a $Co_3V_2O_8$ nanoarray (CoVO@NF) as a base material and performed nitridation and phosphorization treatments to synthesize CoN/VN@NF and P-CoVO@NF materials as both cathode and anode catalysts, respectively. They have proposed that the nitrogen anions upregulate the d-band centre (ε_d) of Co and V to optimize the energy barrier for improving HER activity, and the phosphate anions downregulate the corresponding ε_d to favour the deprotonation of oxygen-containing intermediates during the OER. Their AEMWE cell achieved a current density of 500 mA cm^{-2} at a voltage of 1.76 V and maintained a stable operation for 1000 hours in 1 M KOH electrolyte at 70 °C with only a 1.01% voltage degradation.[69]

4.3. Metal sulfides

Transition metal-based sulfides have been widely studied for alkaline OER/HER applications in the past decades. However, only a limited number of studies have reported their catalytic performance in AEMWE applications. Nonetheless, in general, metal sulfides often perform better in the HER than related hydroxide or oxide materials. This enhancement arises from the higher polarizability of sulfur relative to oxygen, which increases the electron density around the metal centre and optimizes the charge distribution to favour the HER process. The metal sulfides are usually derived from their corresponding metal oxides or hydroxides. In a relevant study, Park *et al.* derived Co_3S_4 nanosheets over NF by direct sulfurization of Co_3O_4 nanosheets over NF. They have observed an increased HER activity of Co_3S_4/NF compared to Co_3O_4/NF in a three-electrode system. Furthermore, they have utilized this Co_3S_4/NF material as a cathode catalyst and CuCo-MMO as an anode catalyst to study single-cell AEMWE performance. They achieved a current density of 431 mA cm^{-2} with cell voltage 2.0 V at 40–45 °C.[118] The metal sulfides can also be derived from MOFs to tune the morphology of the material. In a recent study, Choi *et al.* employed an MOF-derived approach to fabricate Co-incorporated NiS_2 (MD-Co/NiS_2) as an HER electrocatalyst. The resulting MD-Co/NiS_2 retained the original spherical morphology of the MOF precursor, exhibited an increased surface area, and showed improved HER activity in a three-electrode system. When applied as a cathode catalyst in AEMWE, the device achieved a current density of 1 A cm^{-2} at 1.97 V and demonstrated stable operation for 50 hours at 0.5 A cm^{-2} and 70 °C.[59] In another morphology-driven approach, Devarayapalli *et al.* embedded CdS nanoparticles in a zeolite imidazole framework (ZIF-67). The resulting CdS@ZIF-67 nanocomposite, employed as an anode catalyst, delivered a cell potential of 1.85 V at a current density of 1 A cm^{-2} compared to the ZIF-67 material, which required 1.95 V for the same result at 60 °C.[119] For the OER, metal sulfides typically act as pre-catalysts that undergo *in situ* transformation into catalytically active oxyhydroxide phases. For example, Khan *et al.*

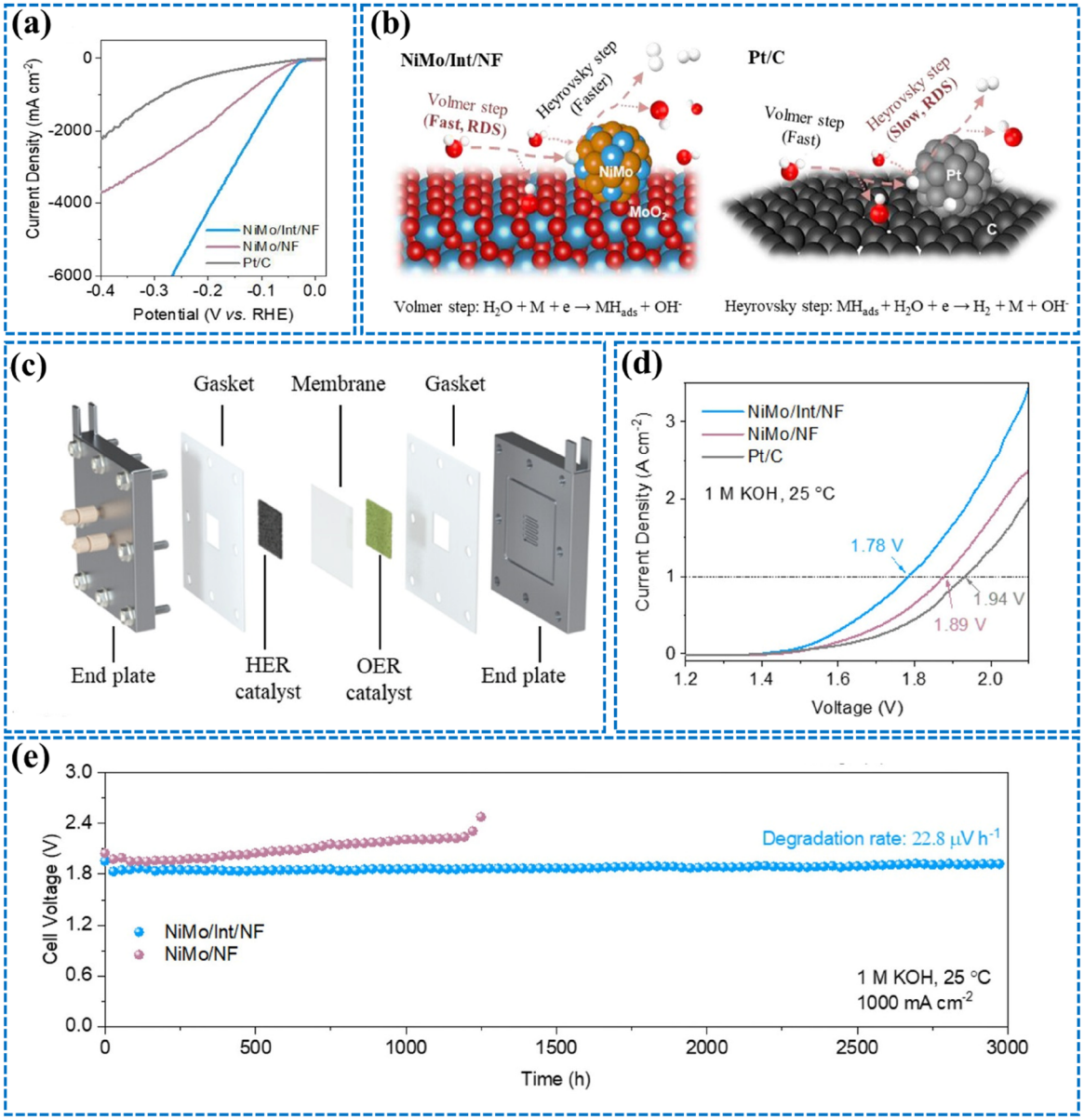

Fig. 5 (a) Polarization curves of NiMo/Int/NF, NiMo/NF, and Pt/C in 1 M KOH; (b) proposed schematic HER mechanism in NiMo/int/NF and Pt/C; (c) schematic of the AEMWE device; (d) polarization curves of CAPist-L1//NiMo/Int/NF, CAPist-L1//NiMo/NF, and CAPist-L1//Pt/C; (e) stability measurements at 1000 mA cm^{-2}.[117] Reprinted with permission from ref. 93. Copyright 2025 Wiley-VCH.

synthesized Co–$FeCo_8S_8$ material using an oriented solid phase synthesis (OSPS) method and performed electrochemical activation to obtain the final catalyst, Co–FeCoOOH. Their proposed method enabled a mechanically strong interface, rapid interfacial charge transfer, and fast bubble evolution under fluctuating working conditions (at constant and fluctuating current densities of 20, 100, 500 mA cm^{-2}). As a result, the AEMWE assembled with the Co–FeCoOOH as an anode catalyst needed a cell voltage of 1.79 V at 1.0 A cm^{-2} with 410 hours of stability at 500 mA cm^{-2}.[66]

The catalytic prominence of Ni and Fe is also reflected in their sulfide-based systems. Also, the utilization of NF as a robust, highly conductive substrate facilitates the direct growth of these catalysts and substantially enhances their overall electrochemical performance. Chanda *et al.* studied NiFeS nanosheets that were immobilized on Ti_3C_2 MXene-decorated nickel foam (Ti_3C_2 MXene/NF) for OER and HER processes and also for AEMWE application.[74] Similarly, Kumar *et al.* utilized NF as a substrate and developed MoS_2–Ni_3S_2/NF as both an anode and a cathode catalyst for AEMWE application.[120] These studies demonstrated the potential of metal sulfides as both anode and cathode catalysts for AEMWE application.

4.4. Metal phosphides

Metal phosphides have been extensively investigated as catalyst materials for the HER and OER in alkaline media. Phosphorus

displays strong electronic interactions with metal centres and modulates their d-band states *via* d–p hybridization to optimize the adsorption–desorption kinetics of the key reaction intermediates. In the HER, this electronic modulation facilitates water dissociation for accelerated hydrogen evolution, while in the OER, these materials generally undergo surface reconstruction to form catalytically active metal oxyhydroxides. Consequently, these materials find their application in water electrolysis, as demonstrated by various research groups in the past decades.[121,122] For AEMWE applications, metal phosphides are majorly utilized as HER catalysts. For instance, Guo *et al.* studied a series of NiFeP materials that were synthesized on AEMs *via* a facile Pd-catalyzed electroless deposition method. The optimized $Ni_{0.79}Fe_{0.08}P_{0.13}$ electrocatalyst showed superior HER performance, comparable to Pt/C in an AEMWE device fed with 1.0 M K_2CO_3 solution.[123] In another study, Kim *et al.* studied NiCoP material as an HER catalyst along with bare NiP and CoP materials, where NiCoP showed superior HER activity compared with the bare materials. This performance enhancement was attributed to the near 1 : 1 balance between phosphide and phosphate in the material. They have achieved 1 A cm^{-2} current density at 1.88 V with 100 hours of stability with a minimal degradation rate of 0.21 mV h^{-1} in a single-cell AEMWE device with a $Ni_{28}Co_{62}P_{10}$/CP cathode and Ni_2Fe_1/SS anode.[124] Apart from the introduction of Fe and Co in NiP materials, B and V doping of NiP materials is also reported for AEMWE applications. Zhao *et al.* reported B and V co-doped in NiP material as a cathode catalyst in alkaline and seawater electrolysis. They have utilized an asymmetric feeding mode for seawater electrolysis (seawater at the cathode and 1 M KOH at the anode side) to avoid a chloride oxidation reaction at the anode side and achieved a decent stability of 30 hours at 0.5 A cm^{-2} current density.[125] In addition, CuCoP material was also reported by Guo *et al.* as a cathode catalyst for AEMWE application.[126]

In addition to transition metals in metal phosphides, the presence of trace amounts of lanthanide metal can boost the catalytic performance. Zhang *et al.* demonstrated a Ce-doped Fe_2P/NiCoP hybrid pre-catalyst that underwent surface reconstruction into highly active (oxy)hydroxide species during the OER with the help of more oxyphilic Ce metal ions. The synthesis procedure of the pre-catalyst is shown in Fig. 6a, where they have used NF as a substrate template for the direct growth of the material. They have observed that the pre-catalyst underwent a controlled surface reconstruction into Ce–FeOOH/NiCoP during the OER with significantly enhanced charge and mass transfer, and reduced the energy barriers for the *OH formation, and this was supported by density functional theory (DFT). They have utilized $Ce_{0.1}Fe_2P$/NiCoP@NF as an anode and homemade $Ce_{0.1}$–CoP/Ni_3P@NF as a cathode to form the MEA and tested it in a customized AEMWE electrolyzer, as illustrated in Fig. 6b and c. The AEM electrolyzer delivered a current density of 1.0 A cm^{-2} at a low cell voltage of 1.812 V and outperformed the benchmarked RuO_2/NF(+)||Pt/C/NF(−) system (2.035 V at 1.0 A cm^{-2}) at 60 °C in 1.0 M KOH solution (Fig. 6d). Furthermore, it sustained a stable operation at 1.0 A cm^{-2} for 579 hours without significant degradation, as shown in Fig. 6e.[57] Furthermore, advanced heterostructure or nanocomposite materials with corresponding hydroxides or sulfides also attracted attention for their versatile electronic and physical properties that favor these gas evolution reactions. Several notable studies, like the mesoporous Ni_2P@$FePO_xH_y$ pre-electrocatalyst studied as an anode material by Meena *et al.*,[127] nickel copper phosphide–nickel sulphide (NCP-NS) as both anode and cathode material by Singh *et al.*,[128] and maple leaf-shaped porous Ni_2P/Ni_7S_6 as an anode by Wang *et al.*,[129] demonstrated industrial-level AEMWE performance.

The use of self-supported electrodes, such as catalysts directly grown on NF, is also widely adopted, as NF not only serves as a structural support but also functions as a GDL within the AEMWE cell. It is therefore important to understand NF and Catalyst@NF's hydrophilic and aerophobic nature towards these gas evolution reactions. Clearly, materials with a highly hydrophilic and aerophobic nature are favourable for these reactions. In this regard, Wan *et al.* developed an $Fe_{0.2}Ni_{0.8}$–$P_{0.5}S_{0.5}$ material, along with bare material Ni–$P_{0.5}S_{0.5}$ over NF, and studied their hydrophilic and aerophobic natures. As shown in Fig. 6f, the contact angles of NF, Ni–$P_{0.5}S_{0.5}$ and $Fe_{0.2}Ni_{0.8}$–$P_{0.5}S_{0.5}$ are 86.1°, 52.9° and 0°, respectively. This demonstrates that the design of the nano-island arrays on the NF surface is beneficial for the electrode's wettability, and $Fe_{0.2}Ni_{0.8}$–$P_{0.5}S_{0.5}$ has superhydrophilic properties. Furthermore, the contact angles for gas bubbles of 72.8, 138.2, and 142.3° for NF, Ni–$P_{0.5}S_{0.5}$, and $Fe_{0.2}Ni_{0.8}$–$P_{0.5}S_{0.5}$, respectively, indicated the superaerophobicity of the $Fe_{0.2}Ni_{0.8}$–$P_{0.5}S_{0.5}$ electrode. Therefore, effective reactant transportation and product removal benefited their developed catalyst, which they employed as both anode and cathode for AMEWE application (Fig. 6g). They have reported a robust performance of their system with a requirement of 2 V cell voltage at 2.5 A cm^{-2} current density and long-term 300-hour stability at 1 A cm^{-2} current density with a degradation rate of 0.08 mV h^{-1} at 60 °C in 1 M KOH.[71]

4.5. Metal alloys

Transition metal alloys hold a promising future as non-precious catalysts for the OER and HER in AEMWE applications. Recent studies utilized Ni, Fe, Co, Cr, Mn, Mo, and their alloys as catalyst materials for AEMWE studies.[63,72,130] For instance, Lee *et al.* studied Fe–Co–Ni ternary amorphous catalyst as an anode catalyst,[131] Yang *et al.* demonstrated several multilayer engineered NiFeM (M: Co, Mn, and Cu) materials as anode catalysts,[64] Wang *et al.* reported a NiCoFeCrMn high-entropy alloy as an anode catalyst,[132] and Yeo *et al.* investigated a NiMo/Co-nanowire (NW)/carbon paper (CP) catalyst as a cathode material for AEMWE.[61]

Surface reconstruction during the OER process is a common phenomenon, and alloy-based materials also undergo the same process. However, limited surface construction often restricts the utilization of active sites on the MEA, which results in limited performance. Thus, the performance can be enhanced by bulk transformation to achieve the maximum number of active sites for the reaction. A study by

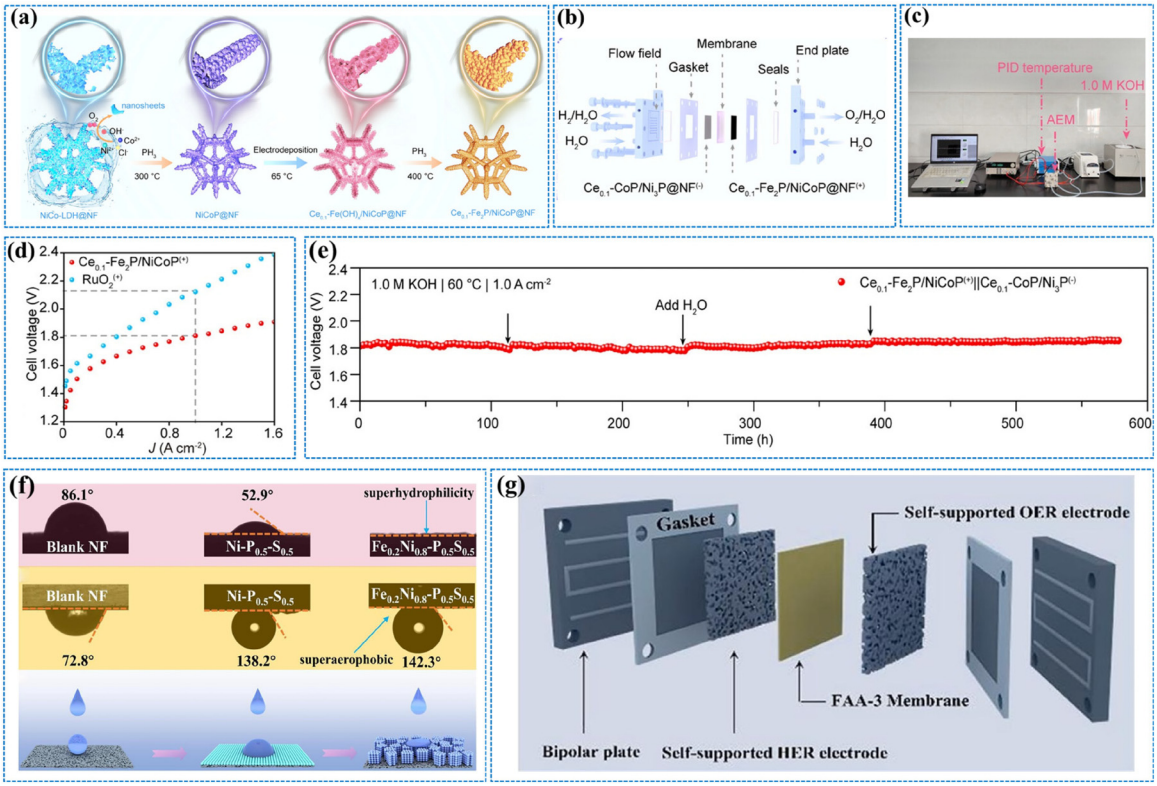

Fig. 6 (a) Schematic illustration of the $Ce_{0.1}$–Fe_2P/NiCoP@NF preparation process; (b) schematic illustration of AEMWE electrolyzers; (c) photograph of an AEMWE platform; (d) *J*–*V* curves of $Ce_{0.1}$–Fe_2P/NiCoP(+)||$Ce_{0.1}$–CoP/Ni_3P(–) and RuO_2@NF(+)||Pt/C@NF(–) at 60 °C; (e) chronopotentiometry of the electrolyzer at 1.0 A cm^{-2} (60 °C, 1.0 M KOH).[57] Reprinted with permission from ref. 107. Copyright 2025 Wiley-VCH. (f) Static water contact-angles, bubble contact angle measurements, and schematic diagram for the transformation of hydrophobic/hydrophilic blank NF, Ni–$P_{0.5}S_{0.5}$ and $Fe_{0.2}Ni_{0.8}$–$P_{0.5}S_{0.5}$ electrodes; (g) schematic component of an AEMWE for testing $Fe_{0.2}Ni_{0.8}$–$P_{0.5}S_{0.5}$//$Fe_{0.2}Ni_{0.8}$–$P_{0.5}S_{0.5}$ catalyst systems.[71] Reprinted with permission from ref. 108. Copyright 2022 Elsevier.

Chen *et al.* showed that the introduction of Mo in a NiFe alloy results in complete surface reconstruction during CV activation *via* Mo leaching with the additional benefit of the presence of cationic vacancies in the structure. The bare NiFe alloy, on the other hand, had limited surface reconstruction (Fig. 7a). As a result, V_{Mo}-NiFe showed better OER performance than bare NiFe. In an AEMWE cell setup with V_{Mo}-NiFe as an anode catalyst the current density of 1.0 A cm^{-2} was achieved at 1.71 V at 60 °C in 1 M KOH. The stability study with continuously changing operating conditions at different current densities and a static current density of 1 A cm^{-2} demonstrated the robust stability of the system (Fig. 7b and c).[133]

Catalyst degradation over time is a serious issue for the practical implementation of AEMWE for hydrogen generation. In a compact cell with a two-electrode system, it is usually difficult to monitor the cause of the degradation of the performance.[134] NiMo-based materials are now widely used as cathode materials for AEMWE, and therefore monitoring and resolving the degradation of NiMo-based cathodes under intermittent operation is necessary. To deal with this, Jeon *et al.* developed an AEMWE cell integrated with a reference electrode with an extended anion exchange membrane to ionically connect the MEA to an external reference electrode chamber, as shown in Fig. 7d. The external chamber housed a reversible hydrogen electrode, immersed in 1 M KOH, and connected ionically to the MEA through the extended membrane region, which functioned as a Luggin capillary to sense the electric field between planar electrodes (Fig. 7e). They have used an MEA with a Ni_3Mo cathode and carbon-encapsulated Ni_3Mo@C60 cathode to study their degradation. Their study revealed that MEAs with Ni_3Mo cathodes exhibited significant degradation, whereas the Ni_3Mo@C60 cathode exhibited remarkable durability under the same conditions. The irreversible transformation of HER-active metallic Ni_3Mo into HER-inactive hydroxides during OCV periods was evidenced during the continuous rise in cathode potential and was considered the primary source of degradation (Fig. 7f and g). The conversion of metallic Ni_3Mo into its hydroxide phase involves substantial volumetric expansion. However, in Ni_3Mo@C60 catalysts, the surrounding carbon shells sterically constrain this expansion, thereby inhibiting the oxidative transformation from metal to hydroxide. Integrating a reference electrode into the AEMWE therefore enabled a precise decoupling of overvoltage contributions, provided critical insights into degradation mechanisms, and allowed a rigorous evaluation of catalyst durability under practical operating conditions.[135]

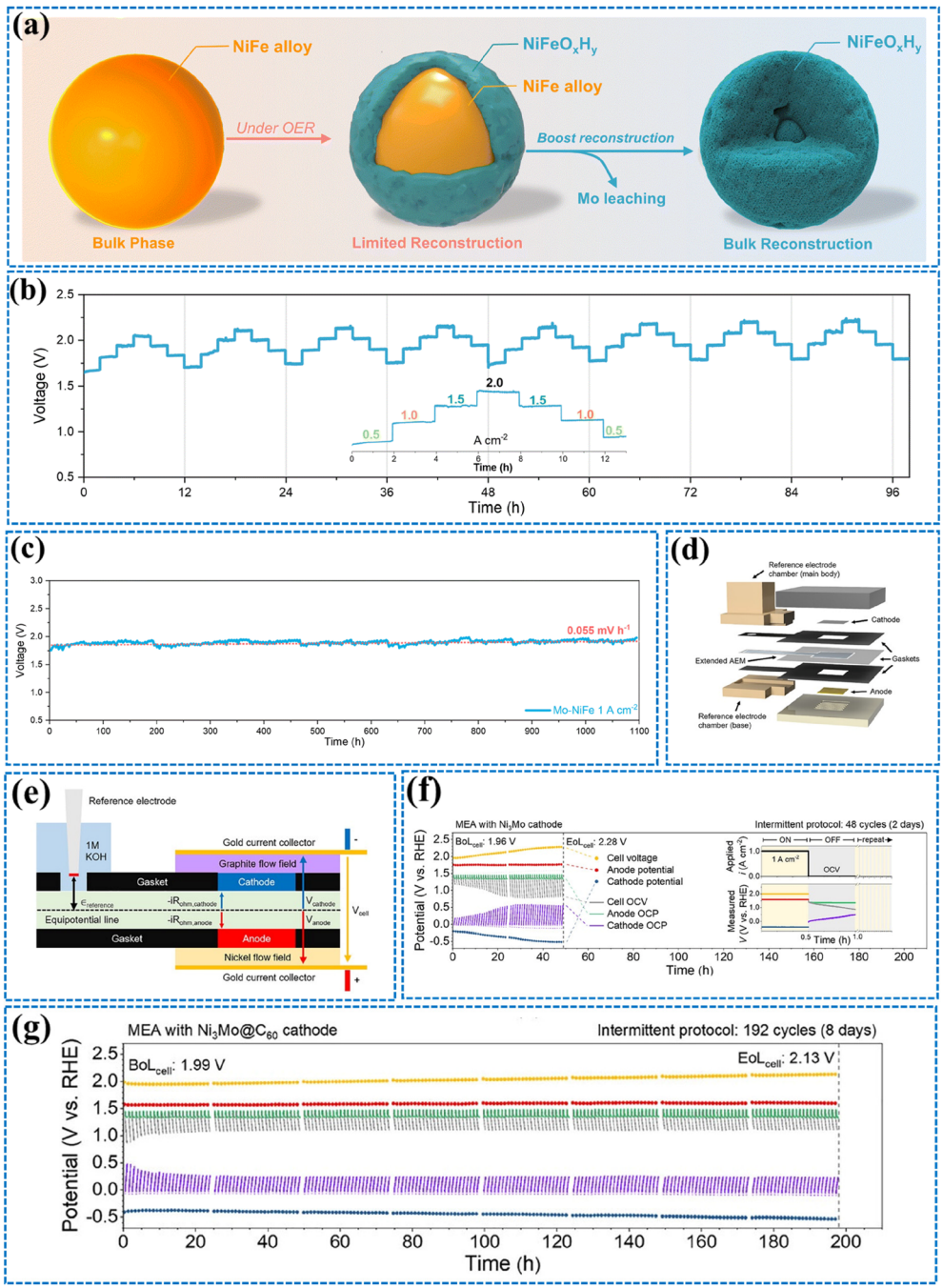

Fig. 7 (a) Schematic of catalyst reconstruction; long-term durability of the Mo-NiFe-based AEMWE recorded under (b) different current densities and (c) a constant current of 1.0 A cm^{-2}.[133] Reprinted with permission from ref. 119. Copyright 2025 Royal Society of Chemistry. (d) Exploded view of AEMWE integrated with a reference electrode; (e) schematics showing the working principle behind the sensing of the electric field between the cathode and anode by the reference electrode; cell voltage and electrode potentials at 1 A cm^{-2} and under an open circuit during an intermittent protocol using (f) Ni_3Mo and (g) Ni_3Mo@C60: the inset figure in (f) indicates an intermittent protocol used to test MEAs, consisting of repeated cycles of 30 min of chronopotentiometry at 1 A cm^{-2} and 30 min of OCV.[135] Reprinted with permission from ref. 121. Copyright 2025 Wiley-VCH.

4.6. Metal organic frameworks

The increasing popularity of MOF as OER catalysts has gained significant attention from researchers. Their tuneable composition with transition metal ions (Ni, Co, Fe, *etc.*) and organic ligands leads to large specific surface areas and abundant pore structures, offering an advantage towards the facile OER process. Recent studies have demonstrated their application in AEMWE also as an anode material. Like other catalysts, MOF materials also act as a pre-catalyst for the OER process, and owing to the presence of weak coordination bonding, they undergo phase transitions into high-valency metal oxyhydrox-

ides at high voltage. Recently, Li *et al.* demonstrated the construction of Ni(Fe)OOH for the OER from a NiFe-MOF material, where benzene-1,4-dicarboxylic acid was used as an organic linker to prepare the NiFe-MOF. The complete structural reconstruction was confirmed *via* post-activation XRD and Raman studies. The presence of Fe caused lattice distortion, resulting in the elongation of Ni–O bonds in the Ni(Fe)OOH with oxygen vacancies. They studied Ni(Fe)OOH for AEMWE as an anode catalyst against the $NiMoO_x$ cathode catalyst and showed more than 300 hours of stability at 1 A cm^{-2} current density.[68] Another study by Lin *et al.* showed the structural reconstruction of B-MOF-Zn–Co to B-doped CoOOH for the facile OER process. They have achieved a current density of 1 A cm^{-2} at 2.04 V using B-MOF-Zn–Co as an anode catalyst.[136] Similarly, Zhou *et al.* reported a D/CoFe-MOF catalyst that underwent stepwise activation during the OER, progressing from the bare MOF state to an intermediate α-FeOOH state, and finally to an OER-active CoFeOOH phase. Theoretical study showed the decreased Co–OOH bond length and enhanced electron localization on adsorbed OOH* species, which resulted in good OER activity. Their AEMWE cell achieved a current density of 1 A cm^{-2} at 1.69 V and maintained a long-life stability for 300 hours with negligible variation at 60 °C in 1 M KOH.[137]

To have the overview of the performance benchmarks, the details of the developed transition metal-based only anode catalysts, only cathode catalysts, and both anode/cathode catalysts for AEMWE application are summarized in Tables 2–4. As observed from the literature, the major focus was found to be on anode catalyst development. However, cathode catalyst development (alternative to a Pt catalyst) is also necessary. Contemporary research needs more focus to develop highly efficient and cheap cathode catalyst materials.

5. Challenges and future prospects

Although AEMWE is still in its infant stage, significant achievements have been made in the development of the components of the MEA, *i.e.*, catalyst materials, membranes, and gas diffusion layers. These advancements have enabled pilot-scale demonstrations in which single-cell AEMWEs achieve current densities approaching 1 A cm^{-2} at low operating voltages with promising stability. Transition metal-based cheap materials are being utilized as high-efficiency anode and cathode catalysts. In parallel, suitable membrane developments are also in progress. These developments have brought the technology closer to practical implementation. Standing at this stage, it is crucial to understand some of the crucial challenges that need to be solved in order to achieve high-performance AEMWE for hydrogen production.[138]

The challenges can be broadly categorized into two classes; one is technical, and the other is economic. Technical challenges include catalytic efficiencies, interfacial issues, membrane durability, MEA's configuration, and operational conditions. Economic challenges are obviously the costs related to the production of catalysts, membranes, and other components. A critical analysis of the technical aspects is outlined below.

5.1. Catalytic efficiency and stability

These are of the utmost importance for high-performance AMEWE process. However, catalyst degradation or the formation of a non-conductive passive layer drastically reduces the catalyst's performance, especially at high current density. It is common for catalysts to undergo surface reconstruction during reactions, which can be monitored *via in situ* studies.[139–141] Therefore, a careful catalyst design with suitable properties for the generation of highly dense active sites with good conductivity during the reaction is highly desirable to achieve a high current density. To deal with this challenge, *operando* characterization approaches are effective to study the material's property during the reaction. Post this, careful engineering is desirable to mitigate the possible degradation issues.

Many studies utilized Nafion as ionomer, which is a cation exchange ionomer.[119,142] This creates a barrier for the HO^- ion to come close to the catalyst as the ionomer suppresses the catalyst's exposure to HO^- ions. This leads to a partial performance loss of the catalyst. Therefore, an anion exchange ionomer is a better choice for this kind of operation. Furthermore, the ionomer–catalyst ratio impacts the overall performance of the catalyst. Excess ionomer would lead to blockage of the catalyst active site and less ionomer content would to poor binding of the catalyst with the membrane or GDL. Therefore, optimization of the ionomer–catalyst ratio is highly desirable.

As the discussed catalysts usually perform well in mild or moderate KOH solutions, as a future target, pure-water activation and impure water activation (such as tap water, pond water, river water, or seawater) could add more value to this technology. For large scale hydrogen production, a direct use of natural water would be highly beneficial. This of course requires a highly active catalyst that can activate water molecules in mild conditions. As pure water provides extremely low ionic conductivity, the catalyst itself must possess high intrinsic conductivity with superhydrophilicity. This could be achieved *via* alloying, nanostructure and interfacial engineering of transition metal-based catalysts. Addressing this challenge would substantially improve both the cost-effectiveness and scalability of hydrogen production.

Recent studies highlight that many catalysts are reported for water electrolysis where testing conditions were used either in three-electrode setups (study of half-cell reactions, *e.g.*, only OER or HER) and/or simply in a two-electrode system in an alkaline medium at room temperature.[18,82,87] Although these studies are important for catalyst development, the vast utilization of these developed catalysts in AEMWE is lacking currently. Therefore, it is necessary to test these catalyst materials on an industrial scale to make the transition faster. Furthermore, several testing protocols in the three-electrode system need to be relevant for practical electrolyzer operation,

Table 2 Comparison of AEMWE performance of reported anode catalyst materials (here, SSE = self-supported electrode, NM = not mentioned)

Anode catalyst	Cathode catalyst	Membrane	MEA type/binder	Electrolyte/ temperature (°C)	Flow direction/ flow rate (mL min^{-1})	Performance (j (A cm^{-2})/E (V))	Stability duration (h)/j (A cm^{-2})	Ref.
NiCo@FeNi LDH	Pt/C	QAPPT	CCM/QAPPT ionomer	1 M KOH/60	Both sides/NM	3.61/2.0	700/1.0	47
FCNal/NF	Pt/C/NF	FAA-3-50	CCS/binder free	30 wt% KOH/80	Both sides/200	1.0/1.73	36/1.0 or 2.0	63
NiFeMn	PtRu/C	Versogen	CCS/TP855	1 M KOH/80	Both sides/0.35	2.0/1.7	24/0.5	64
CdS/ZIF-67	Pt/C	Fumapem, FAA-3–50	CCS/Nafion	1 M KOH/60	Both sides/2	1.0/1.85	Not performed	119
Co@MXene	PtRu/C	Xion Pention-72–15CL	CCS/TMA-70 ionomer	1 M KOH/80	Both sides/NM	2.11/1.8	700/0.2	65
$Co_{2.8}W_{3.8}$–NiFe LDH	Pt/C	Sustainion X37-50	SSE/binder free	1 M KOH/60	Both sides/NM	1.0/1.86	300/1.0	94
Co_4Fe_3@N	Pt/C	PiperION-A15R, 5 μm, Versogen	CCS/Nafion	1 M KOH/60	Anode side/100	0.5/NM	600/0.5 & 0.75	142
Co–$FeCo_8S_8$	FeMoNi	Sustanion X37-50 Grade RT	SSE/binder free	1 M KOH/60	NM/NM	1.0/1.79	410/0.5	66
$Cu_{0.5}Co_{2.5}O_4$	Pt/C	X37-50 Grade T	CCS/PTFE	1 M KOH/50	NM/50	1.3/1.8	100/0.4	115
$Cu_xCo_{3-x}O_4$	Ni/CP	Fumapem FAA-3-50	SSE/binder free	1 M KOH/40	Both sides/2	0.1/2.0	18/0.025	67
NiFe/C	PtRu/C	XL20-rPNB-LY100	CCS/TMA-70 ionomer	1 M NaOH/80	Both sides/NM	0.2/1.8	1100/0.2	143
NiFe-BTC-GNPs MOF	$MoNi_4/MoO_2$	FAA-3-PK-130 (Fumatech)	CCS/ionomer	0.1 M KOH/70	Both sides/NM	0.540/1.85	96/0.01	144
$NiCoO_x$	Pt/C	Sustainion® X-37-50 T	CCS/Nafion	1 M KOH/55	Both sides/90	1.684/2.2	30/0.25	145
La–Sr–Co oxide	PtRu/C	PiperION-A40-HCO_3 (Versogen)	CCS/Nafion	0.1 M KOH/70	Anode side/10	1.0/1.9	20/0.3	146
Ni(Fe) MOF	$NiMoO_x$	PiperIONTM	SSE/binder free	1 M KOH/60	Both sides/NM	0.5/1.67	300/0.5	68
$Ni_{0.6}Co_{0.2}Fe_{0.2}$	Pt/C	Fumapem-3-PE-30	CCS/Fumion FAA-3	1 M KOH/50	NM/250	1.5/2.0	50/0.01	147
Ni_2P@$FePO_xH_y$	$MoNi_4/MoO_2$	Sustainion® X37-50	CCS/anion ionomer	1 M KOH/60	Cathode side/NM	1.0/1.84	72/0.48	127
Ni_2P/Ni_7S_6	Pt/C	Fumasep FAA-3-50	CCS, SSE/not mentioned	1 M KOH/75	Both sides/NM	1.0/1.88	140/1.0	129
CAPist-S1	$MoO_2/MoNi_4$/NF	PiperION-A	SSE/binder free	1.0 M KOH + seawater/rt	Anode side/NM	1/1.91	700/1.0	93
NiCoFeCrMn	Pt/C	X37-50 Grade T	CCS/not mentioned	1 M KOH/60	NM/NM	2/2.10	100/1.0	132
Mo–NiFe	Pt/C	PiperION-A40R-HCO_3	CCS/PiperION-A5-HCO_3 ionomer	1 M KOH/60	Both sides/NM	1/1.71	1000/1.0	133
NiFeOOH/N-CFP	$MoNi_4/MoO_2$/NF	Fumatech FAA-3-50	SSE/binder free	Pure water/50	Cathode side/NM	1/1.88	240@2 V	108
$NiMn_2O_4$	Pt/C	FAA-3-50	CCM/FAA-3 shredded film	1 M KOH/80	Anode side/4	0.53/2	1000@1–1.8 V	113
$NiCo_2O_4$/CNF	Pt/C	Fumasep FAA-3-50	CCS/anion ionomer	6 M KOH/50	Anode side/4	0.181/1.8	Not performed	114
Fe–Co_3–Ni	Pt/C	FAA-3-50, FuMaTech	CCM/Nafion 117	1 M KOH/60	Both sides/NM	2.0/1.89	100/0.5	131
z-NiFe	$MoNi_4/MoO_2$	PAP-TP-85	SSE/binder free	1 M KOH/80	Both sides/30	7.86/2.0	14 000/1	100

Table 3 Comparison of AEMWE performance of reported cathode catalyst materials (here, SSE = self-supported electrode, NM = not mentioned)

Anode catalyst	Cathode catalyst	Membrane	MEA type/binder	Electrolyte/ temperature (°C)	Flow direction/ flow rate (mL min^{-1})	Performance (j (A cm^{-2})/E (V))	Stability duration (h)/j (A cm^{-2})	Ref.
NiFe-LDH	CoFe@HNCS20	X37-50 Grade T	CCS/Nafion and Fumion FAA-3	1 M KOH/55	NM/50	0.5/1.808	112/0.5	148
IrO_2	MD-Co/NiS_2	Sustainion X37-50	CCS/Nafion	1 M KOH/70	Both sides/5	1/1.97	50/0.5	59
Ni_3Fe_1/SS	$Ni_{28}Co_{62}P_{10}$/CP	PiperION	CCS (*via* electrodeposition)	1 M KOH/80	Anode side/3	1/1.88	100/1.0	124
NFP	Ni_3N@W_5N_4	Fumasep FAA-3-50	CCM/Fumion FAA-3-SOLUT-10	1 M KOH + seawater/60	Cathode side/NM	1/2.12	30/1.0	60
IrO_2/CP	NiMo/Co-NW/CP	Sustainion X37-50 Grade RT	CCS/Nafion	1 M KOH /80	Both sides/(catholyte -2 and anolyte -20)	1.52/2	Not performed	61
Ir black	NiCu MMO	Fumapem-3-PE-30	CCS/Fumion FAA-3-SOLUT-10	1 M KOH/50	Both sides/250	1.85/2	Not performed	33
CoNi-LDH-130	WO_3@CoNi-LDH-130	PVA/PVP/SiO_2	CCS/SEBS and PVDF	1 M KOH/50	Anode side/50	0.1/1.53	1000 @ 1.42 V	50
IrO_2/CP	CuCoP/CP	Sustainion® 37	CCS (*via* electrodeposition)	1 M KOH/50	From cathode/10	0.70/1.92	Not performed	126
NiFe oxyhydroxide	$NiFeO_x$	FAA-3-50	CCS/FAA-3-Br	1 M KOH/70	Both sides/1	1.48/2.05	40/0.5	58
$Cu_{0.81}Co_{2.19}O_4$	3-Co_3S_4 NS/NF	Sustainion® X37-50	CCS (*via* electrodeposition)	1 M KOH/48	Anode side/25	0.431/2	12/0.5	118
NiFeOOH	B, V-Ni_2P	X37-50	CCS/binder free	1 M KOH/55	Both sides/NM	1/1.92	100/0.5	125

such as electrolyte composition, pH, and temperature, along with mass-loading optimization, activity, and long-term stability testing at meaningful current densities.

5.2. Interfacial compatibility

This issue arises from poor adhesion and mismatched interfaces between the catalyst and membrane, which can impede electron and mass transfer across the MEA and consequently limit cell performance.[31] Such problems often originate from improper MEA fabrication methods or due to the incompatibility of membrane–ionomer–catalyst. Therefore, ensuring intimate contact and optimized structural integration between the catalyst and membrane easily mitigates this challenge for enhanced AEMWE performance. This requires case studies with membrane and ionomer variants to understand and solve the issue. Also, as discussed before, an interlocking strategy to fabricate the MEA is a potential solution to minimize the interfacial incompatibility, requiring no need for an ionomer.

5.3. Membrane conductivity and durability

The conductivity and durability of the AEM have a huge impact on AEMWE's performance. Unlike PEM, AEMs are less durable, and therefore significant research effort to develop highly efficient membranes is necessary. In order to get high conductivity and close contact of the electrodes, the membrane must be thin, but thin membranes degrade fast. On the other hand, thick membranes are durable but less conductive. Hence, a thin membrane is highly desirable with good stability. Furthermore, AEMs face degradation issues under high pH conditions and elevated temperatures.[154] Therefore, a clear objective is a trade-off through advanced material design, such as chemically robust backbones, improved ion-exchange groups, and composite strategies, which is imperative. In parallel, the cost of production needs to be reduced for affordable marketing.

5.4. MEA fabrication

MEA fabrication, whether *via* a CCS, CCM, or ordered interlock strategy, has a huge impact on AEMWE's performance. Although multiple fabrication approaches have been reported in the literature, a universally accepted benchmark for optimal MEA preparation has yet to be established.[31,47] Contemporary research should focus on identifying fabrication strategies that maximize the efficiency, durability, and scalability of AEMWE devices.

5.5. Operational conditions and standardized testing

In the past, the testing of AEMWE has been evaluated under diverse operational conditions, including electrolyte types (pure water, alkaline water, seawater, *etc.*), operating temperatures (25–80 °C), feeding methods (anode feeding, cathode feeding, and dual feeding modes), and flow rates (1–500 mL min^{-1}). However, as highlighted by Titheridge *et al.*, building a consistent relationship between these variables and cell performance is a challenge as of now, due to the lack of standardized testing protocols. Hence, they have proposed standar-

Table 4 Comparison of AEMWE performance of reported bifunctional anode/cathode catalyst materials (here, SSE = self-supported electrode, NM = not mentioned, rt = room temperature)

Anode catalyst	Cathode catalyst	Membrane	MEA type/binder	Electrolyte/ temperature (°C)	Flow direction/flow rate (mL min^{-1})	Performance (j (A cm^{-2})/E (V))	Stability duration (h)/j (A cm^{-2})	Ref.
$VCoCO_x$@NF	$VCoCO_x$@NF	FAA-3-50	SSE/binder free	Pure water/45	NM	0.2/2.10	12/0.25	149
$Co_{6.5}Fe_{3.5}O_xH_y$/TP	$Co_{6.5}Fe_{3.5}O_xH_y$/TP	Sustainion® X37-50	SSE/binder free	1 M KOH/50	Both sides/20	0.615/2.0	50/0.6	70
$Fe_{0.2}Ni_{0.8}P_{0.5}S_{0.5}$	$Fe_{0.2}Ni_{0.8}P_{0.5}S_{0.5}$	FAA-3-50	CCS/FAA-3 ionomer	1 M KOH/60	NM/50	2.5/2.0	300/1.0	71
$FeNi_3/FeNiO_x$	$FeNi_3/FeNiO_x$	AT-100	CCS/ polytetrafluoroethylene	1 M KOH/60	NM/200	1.0/1.94	150/0.4	72
NFA-CA	NFA-CA	Sustainion X37-50	SSE/binder free	1 M KOH/60	Both sides/100	1.0/1.56	1000/1.0	150
FCPWP	FCPWP	Sustainion X37-50	CCS/Nafion	1 M KOH/50	Both sides/not mentioned	0.425/1.85	72/0.425	151
NiFe-NiMoP/ZnO	NiFe-NiMoP/ZnO	PiperION	SSE/binder free	1 M KOH/50	Both sides/5	1/1.87	200/0.5	152
MoS_2-Ni_3S_2/NF	MoS_2-Ni_3S_2/NF	Sustainion	SSE/binder free	1 M KOH/not mentioned	Both sides/5	0.02/1.75	48/0.02	153
NiFeS@Ti_3C_2/NF	NiFeS@Ti_3C_2/NF	Sustainion X37–50 RT	SSE/binder free	1 M KOH/50	Both sides/NM	0.401/1.85	35/0.4	74
NCP-NS	NCP-NS	Sustainion™ X37–50	SSE/binder free	1 M KOH/rt	Both sides/0.35	0.23/2.0	300/0.08 to 0.8	128
NiFe-LDH/Ni_4Mo	NiFe-LDH/Ni_4Mo	FAA-3-20	SSE/binder free	1 M KOH/rt	NM/NM	0.1/1.68	150/0.1	107

dized testing protocols for AEMWE to benchmark the overall system configuration.[155] Several other reports and international agencies also highlighted standardized testing protocols for AEMWE for a reliable comparison and to accelerate scale-up.[19,25,156] Following these protocols the performance *vs.* the standardized testing would provide a meaningful solution for future operations.

6. Summary and perspective

In summary, we have provided a concise overview of modern technologies for hydrogen production *via* water electrolysis, with a particular focus on the emergence and significance of AEMWE for cost-effective hydrogen generation. Key components of AEMWE and their operating mechanisms were highlighted to present a comprehensive understanding of the cell architecture. Furthermore, membrane–catalyst compatibility with efficient MEA fabrication strategies was discussed. We provided a detailed analysis of recent advances in non-precious, Earth-abundant catalyst materials investigated over the past decades, emphasizing the critical roles of metal compositions such as Ni and Fe for the OER and Ni and Mo for the HER, as well as their synergistic interactions in replacing PGM catalysts to enhance AEMWE performance. Finally, the current status, challenges, and future prospects were highlighted for the transition from pilot-scale to industrial-level AEMWE applications.

AEMWE holds substantial potential for hydrogen production on an industrial scale, and significant research and development is required to achieve this goal. Therefore, a thorough understanding of a catalyst's property and its degradation mechanism at operating conditions is imperative. The dynamic reconstruction is a common phenomenon that occurs during the reactions and needs to be monitored *via in situ* characterization studies. Pre- and post-study characterization studies are also necessary to understand the same. Along with stability, the activity of the materials needed to be retained during the cell operation, and therefore, catalysts with high conductivity and abundant active sites are necessary. Although this review emphasized the recent catalyst development, the need for membrane development and MEA fabrication has equal importance for the successful implementation of AEMWE technology. Therefore, more focused research should be devoted to the GDL/CL/AEM interfaces to improve MEA performance and operational lifetime.

Author contributions

Suprobhat Singha Roy conceived the original draft idea, conducted the literature survey, constructed the draft and wrote the manuscript. Sreenivasan Nagappan and Prasita Mazumder contributed to writing and revising the manuscript and preparing the figures. Fajar Dhanish C P and Vishesh Vishesh compiled the data presented in the tables and assisted in editing

the figures and manuscript. Subrata Kundu supervised, reviewed, and edited the manuscript.

Conflicts of interest

There are no conflicts to declare.

Data availability

All data related to this study are available from the authors upon request.

Acknowledgements

Suprobhat Singha Roy acknowledges UGC for the fellowship. Sreenivasan Nagappan and Prasita Mazumder wish to acknowledge the Department of Science and Technology (DST) for the Inspire Fellowship. CSIR-CECRI Manuscript number: CECRI/PESVC/Pubs/2025- 147.

References

1 I. Dincer, *Int. J. Hydrogen Energy*, 2012, **37**, 1954–1971.
2 P. P. Edwards, V. L. Kuznetsov, W. I. F. David and N. P. Brandon, *Energy Policy*, 2008, **36**, 4356–4362.
3 M.-N. N. Shafiqah, T. J. Siang, P. S. Kumar, Z. Ahmad, A. A. Jalil, M. B. Bahari, Q. Van Le, L. Xiao, M. Mofijur, C. Xia, S. F. Ahmed and D.-V. N. Vo, *Environ. Chem. Lett.*, 2022, **20**, 1695–1718.
4 W. Li, H. Tian, L. Ma, Y. Wang, X. Liu and X. Gao, *Mater. Adv.*, 2022, **3**, 5598–5644.
5 A. Bazarah, E. H. Majlan, T. Husaini, A. M. Zainoodin, I. Alshami, J. Goh and M. S. Masdar, *Int. J. Hydrogen Energy*, 2022, **47**, 35976–35989.
6 P. Shirvanian, A. Loh, S. Sluijter and X. Li, *Electrochem. Commun.*, 2021, **132**, 107140.
7 H. A. Miller, K. Bouzek, J. Hnat, S. Loos, C. I. Bernäcker, T. Weißgärber, L. Röntzsch and J. Meier-Haack, *Sustainable Energy Fuels*, 2020, **4**, 2114–2133.
8 C. Li and J.-B. Baek, *Nano Energy*, 2021, **87**, 106162.
9 D. Li, A. R. Motz, C. Bae, C. Fujimoto, G. Yang, F.-Y. Zhang, K. E. Ayers and Y. S. Kim, *Energy Environ. Sci.*, 2021, **14**, 3393–3419.
10 S. Li, E. Li, X. An, X. Hao, Z. Jiang and G. Guan, *Nanoscale*, 2021, **13**, 12788–12817.
11 S. Singha Roy, R. Madhu, K. Bera, S. Nagappan, H. N. Dhandapani, A. De and S. Kundu, *ACS Appl. Mater. Interfaces*, 2024, **16**, 5965–5976.
12 J. Wang, X. Yue, Y. Yang, S. Sirisomboonchai, P. Wang, X. Ma, A. Abudula and G. Guan, *J. Alloys Compd.*, 2020, **819**, 153346.
13 K. Pradeep, A. A. Jeffery, A. P. Sundaresan, R. Gunaseelan, S. Rajendran, P. E. Karthik, Y.-H. Ahn and N. C. Sagaya Selvam, *J. Mater. Chem. A*, 2025, **13**, 14510–14539.
14 R. R. Raja Sulaiman, W. Y. Wong and K. S. Loh, *Int. J. Energy Res.*, 2022, **46**, 2241–2276.
15 J. Yang, M. J. Jang, X. Zeng, Y. S. Park, J. Lee, S. M. Choi and Y. Yin, *Electrochem. Commun.*, 2021, **131**, 107118.
16 L. Wan, Z. Xu, Q. Xu, M. Pang, D. Lin, J. Liu and B. Wang, *Energy Environ. Sci.*, 2023, **16**, 1384–1430.
17 C. Van Pham, D. Escalera-López, K. Mayrhofer, S. Cherevko and S. Thiele, *Adv. Energy Mater.*, 2021, **11**, 2101998.
18 S. Sebbahi, A. Assila, A. Alaoui Belghiti, S. Laasri, S. Kaya, E. K. Hlil, S. Rachidi and A. Hajjaji, *Int. J. Hydrogen Energy*, 2024, **82**, 583–599.
19 International Renewable Energy Agency, *Green hydrogen cost reduction: Scaling up electrolysers to meet the 1.5C climate goal*, Abu Dhabi, 2020.
20 G. Tsotridis and A. Pilenga, *EU harmonized protocols for testing of low temperature water electrolysis*, Publications Office of the European Union, 2021.
21 G. Bender, M. Carmo, T. Smolinka, A. Gago, N. Danilovic, M. Mueller, F. Ganci, A. Fallisch, P. Lettenmeier, K. A. Friedrich, K. Ayers, B. Pivovar, J. Mergel and D. Stolten, *Int. J. Hydrogen Energy*, 2019, **44**, 9174–9187.
22 E. K. Volk, M. E. Kreider, S. Kwon and S. M. Alia, *EES Catal.*, 2024, **2**, 109–137.
23 Y. S. Park, J. Jeong, Y. Noh, M. J. Jang, J. Lee, K. H. Lee, D. C. Lim, M. H. Seo, W. B. Kim, J. Yang and S. M. Choi, *Appl. Catal., B*, 2021, **292**, 120170.
24 F. Bartoli, L. Capozzoli, T. Peruzzolo, M. Marelli, C. Evangelisti, K. Bouzek, J. Hnát, G. Serrano, L. Poggini, K. Stojanovski, V. Briega-Martos, S. Cherevko, H. A. Miller and F. Vizza, *J. Mater. Chem. A*, 2023, **11**, 5789–5800.
25 Q. Xu, L. Zhang, J. Zhang, J. Wang, Y. Hu, H. Jiang and C. Li, *EnergyChem*, 2022, **4**, 100087.
26 R. R. Raja Sulaiman, W. Y. Wong and K. S. Loh, *Int. J. Energy Res.*, 2022, **46**, 2241–2276.
27 Q. Lu, X. Yan, W. Guo, G. Li, J. Wang, N. Jiang, X. Wang, T. Ba, P. Liu, J. Zhou, J. Wang, L. Hu, T. Zhou, R. Huang, B. Hu, K. Zhang and Z. Ren, *Nano Res.*, 2025, **18**, 94907252.
28 C. Santoro, A. Lavacchi, P. Mustarelli, V. Di Noto, L. Elbaz, D. R. Dekel and F. Jaouen, *ChemSusChem*, 2022, **15**, e202200027.
29 S. A. Lee, J. Kim, K. C. Kwon, S. H. Park and H. W. Jang, *Carbon Neutralization*, 2022, **1**, 26–48.
30 A. Karmakar, R. Madhu, S. Nagappan, A. De, S. S. Roy, H. N. Dhandapani, A. K. Satheesan, P. Mazumder and S. Kundu, *J. Mater. Chem. A*, 2025, **13**, 19252–19281.
31 L. Titheridge, S. K. Sharma, A. Soisson, C. Roth and A. T. Marshall, *Curr. Opin. Electrochem.*, 2025, **49**, 101607.
32 S. M. Alia and B. S. Pivovar, *J. Electrochem. Soc.*, 2018, **165**, F441–F455.
33 A. Y. Faid, A. O. Barnett, F. Seland and S. Sunde, *Electrochim. Acta*, 2021, **371**, 137837.

34 R. R. Raja Sulaiman, W. Y. Wong and K. S. Loh, *Int. J. Energy Res.*, 2022, **46**, 2241–2276.
35 R. Jervis, N. Mansor, A. J. Sobrido, S. Jones, C. Gibbs, T. P. Neville, J. Millichamp, P. R. Shearing and D. J. L. Brett, *J. Electrochem. Soc.*, 2017, **164**, F1551–F1555.
36 M. Klingenhof, H. Trzesniowski, S. Koch, J. Zhu, Z. Zeng, L. Metzler, A. Klinger, M. Elshamy, F. Lehmann, P. W. Buchheister, A. Weisser, G. Schmid, S. Vierrath, F. Dionigi and P. Strasser, *Nat. Catal.*, 2024, **7**, 1213–1222.
37 K. Lou, L. Xia, J. Friedrich and M. Shviro, *Int. J. Hydrogen Energy*, 2024, **49**, 591–603.
38 Q. Xu, S. Z. Oener, G. Lindquist, H. Jiang, C. Li and S. W. Boettcher, *ACS Energy Lett.*, 2021, **6**, 305–312.
39 J. E. Park, S. Y. Kang, S.-H. Oh, J. K. Kim, M. S. Lim, C.-Y. Ahn, Y.-H. Cho and Y.-E. Sung, *Electrochim. Acta*, 2019, **295**, 99–106.
40 L. Titheridge, S. K. Sharma, A. Soisson, C. Roth and A. T. Marshall, *Curr. Opin. Electrochem.*, 2025, **49**, 101607.
41 M. Klingenhof, H. Trzesniowski, S. Koch, J. Zhu, Z. Zeng, L. Metzler, A. Klinger, M. Elshamy, F. Lehmann, P. W. Buchheister, A. Weisser, G. Schmid, S. Vierrath, F. Dionigi and P. Strasser, *Nat. Catal.*, 2024, **7**, 1213–1222.
42 F. Razmjooei, R. Reißner, A. S. Gago and A. Ansar, *ECS Trans.*, 2019, **92**, 689–702.
43 N. I. Kim, J. Lee, S. Jin, J. Park, J. Jeong, J. Lee, Y. Kim, C. Kim and S. M. Choi, *Small Methods*, 2024, **8**, 2400284.
44 S. Ruck, A. Hutzler, S. Thiele and C. van Pham, *Small Methods*, 2025, **9**, 2401179.
45 I. Galkina, A. Y. Faid, W. Jiang, F. Scheepers, P. Borowski, S. Sunde, M. Shviro, W. Lehnert and A. K. Mechler, *Small*, 2024, **20**, 2311047.
46 P. K. Gangadharan, H. Kuroki, S. Miyanishi, H. Okuyama and T. Yamaguchi, *ACS Appl. Energy Mater.*, 2025, **8**, 10637–10646.
47 L. Wan, J. Liu, D. Lin, Z. Xu, Y. Zhen, M. Pang, Q. Xu and B. Wang, *Energy Environ. Sci.*, 2024, **17**, 3396–3408.
48 T.-H. Kong, P. Thangavel, S. Shin, S. Kwon, H. Choi, H. Lee, N. Park, J.-J. Woo and Y. Kwon, *ACS Energy Lett.*, 2023, **8**, 4666–4673.
49 F.-L. Wang, N. Xu, C.-J. Yu, J.-Y. Xie, B. Dong, X.-Y. Zhang, Y.-W. Dong, Y.-L. Zhou and Y.-M. Chai, *Appl. Catal., B*, 2023, **330**, 122633.
50 S. Prabu, M. Arivazhagan, K.-Y. Chiang, M. R. Pallavolu and T. V. M. Sreekanth, *Chem. Eng. J.*, 2025, **514**, 163266.
51 H. Saada, G. Benoit, J. Dabboussi, C. Lagrost, B. Fabre and G. Loget, *Adv. Mater. Interfaces*, 2025, **12**, 2500305.
52 S. Shin, S. Park, Y. R. Lee, Y. Shin, D. M. Yu, S. J. Yoon, H. Y. Jeong, T. Kim, H. Han, Y. Sung and S. Kim, *J. Am. Ceram. Soc.*, 2025, **108**, e20648.
53 P. Thangavel, H. Lee, T. Kong, S. Kwon, A. Tayyebi, J. Lee, S. M. Choi and Y. Kwon, *Adv. Energy Mater.*, 2023, **13**, 2203401.
54 M. E. Kreider, H. Yu, L. Osmieri, M. R. Parimuha, K. S. Reeves, D. H. Marin, R. T. Hannagan, E. K. Volk, T. F. Jaramillo, J. L. Young, P. Zelenay and S. M. Alia, *ACS Catal.*, 2024, **14**, 10806–10819.
55 S. Koch, J. Disch, S. K. Kilian, Y. Han, L. Metzler, A. Tengattini, L. Helfen, M. Schulz, M. Breitwieser and S. Vierrath, *RSC Adv.*, 2022, **12**, 20778–20784.
56 A. W. Tricker, J. K. Lee, J. R. Shin, N. Danilovic, A. Z. Weber and X. Peng, *J. Power Sources*, 2023, **567**, 232967.
57 F. Zhang, K. Wang, H. Zhang, S. Yang, M. Xu, Y. He, L. Lei, P. Xie and X. Zhang, *Adv. Funct. Mater.*, 2025, **35**, 2500861.
58 J. E. Park, Y.-E. Sung and C. Choi, *J. Mater. Chem. A*, 2022, **10**, 20517–20524.
59 H. Choi, S. Jo, H. Lim, Y.-W. Lee and J. I. Sohn, *Surf. Interfaces*, 2024, **46**, 103987.
60 H. Huang, L. Xu, S. Zuo, Y. Ren, L. Song, C. Zou, X. Wang, J. R. Martínez, K. Huang and H. Zhang, *Angew. Chem., Int. Ed.*, 2024, **64**, e202414647.
61 K.-R. Yeo, H. S. Park, S. Ahn, S. H. Ahn and S.-K. Kim, *Appl. Surf. Sci.*, 2025, **694**, 162842.
62 L. Wu, M. Ning, X. Xing, Y. Wang, F. Zhang, G. Gao, S. Song, D. Wang, C. Yuan, L. Yu, J. Bao, S. Chen and Z. Ren, *Adv. Mater.*, 2023, **35**, 2306097.
63 L. Ma, Z. Wei, X. Meng, Y. Wang, X. Huang, M. Feng, P. He, D. Jia, Y. Zhou and X. Duan, *Chem. Eng. J.*, 2025, **504**, 158217.
64 X. Yang, J. Liang, Q. Shi, M. J. Zachman, S. Kabir, J. Liang, J. Zhu, B. Slenker, M. Pupucevski, N. Macauley, A. J. Kropf, H. Zeng, D. Strasser, D. J. Myers, H. Xu, Z. Zeng, Y. Yan and G. Wu, *Adv. Energy Mater.*, 2024, **14**, 2400029.
65 Y. S. Park, A. Chae, G. H. Choi, S. Ram, S.-C. Lee, S. Bhattacharjee, J. Jung, H. S. Jeon, C.-H. Ahn, S. S. Hwang, D.-Y. Koh, I. In, T. Oh, S. J. Kim, C. M. Koo and A. S. Lee, *Appl. Catal., B*, 2024, **346**, 123731.
66 J. Khan, H. Liu, T. Zhang, X. Kang, Z. Zhang, Y. Dong, S. Li, J. Liu, Q. Yu and B. Liu, *Energy Environ. Sci.*, 2024, **17**, 9435–9442.
67 E. López-Fernández, J. Gil-Rostra, J. P. Espinós, A. R. González-Elipe, F. Yubero and A. de Lucas-Consuegra, *J. Power Sources*, 2019, **415**, 136–144.
68 Y. Li, L. Yang, X. Hao, X. Xu, L. Xu, B. Wei and Z. Chen, *Angew. Chem., Int. Ed.*, 2024, **64**, e202413916.
69 Z. Liang, D. Shen, Y. Wei, F. Sun, Y. Xie, L. Wang and H. Fu, *Adv. Mater.*, 2024, **36**, 2408634.
70 S. Hong, H. Kim, H. W. Jang, S. Y. Kim and S. H. Ahn, *Dalton Trans.*, 2023, **52**, 6324–6330.
71 L. Wan, Z. Xu, P. Wang, P.-F. Liu, Q. Xu and B. Wang, *Chem. Eng. J.*, 2022, **431**, 133942.
72 F. Malaj, A. Tampucci, D. Lentini, L. Brogi, E. Berretti, C. Coletti, S. Forti, A. Rossi and C. Santoro, *Electrochim. Acta*, 2024, **507**, 145109.
73 T. Jiang, X. Jiang, C. Jiang, J. Wang, Y. Danlos, T. Liu, C. Deng, C. Chen, H. Liao and V. Kyriakou, *Adv. Energy Mater.*, 2025, **15**, 2501634.
74 D. Chanda, K. Kannan, J. Gautam, M. M. Meshesha, S. G. Jang, V. A. Dinh and B. L. Yang, *Appl. Catal., B*, 2023, **321**, 122039.

75 A. Karmakar, R. Madhu, S. S. Roy and S. Kundu, in *Multifunctional Electrocatalysts*, Royal Society of Chemistry, 2024, pp. 21–44.
76 D. Eum, B. Kim, J.-H. Song, H. Park, H.-Y. Jang, S. J. Kim, S.-P. Cho, M. H. Lee, J. H. Heo, J. Park, Y. Ko, S. K. Park, J. Kim, K. Oh, D.-H. Kim, S. J. Kang and K. Kang, *Nat. Mater.*, 2022, **21**, 664–672.
77 A. Grimaud, O. Diaz-Morales, B. Han, W. T. Hong, Y.-L. Lee, L. Giordano, K. A. Stoerzinger, M. T. M. Koper and Y. Shao-Horn, *Nat. Chem.*, 2017, **9**, 457–465.
78 S. Anantharaj, S. Kundu and S. Noda, *Nano Energy*, 2021, **80**, 105514.
79 L. Li, X. Cao, J. Huo, J. Qu, W. Chen, C. Liu, Y. Zhao, H. Liu and G. Wang, *J. Energy Chem.*, 2023, **76**, 195–213.
80 L. Han, S. Dong and E. Wang, *Adv. Mater.*, 2016, **28**, 9266–9291.
81 P. Sabatier, *Ber. Dtsch. Chem. Ges.*, 1911, **44**, 1984–2001.
82 D. P. Sahoo, K. K. Das, S. Mansingh, S. Sultana and K. Parida, *Coord. Chem. Rev.*, 2022, **469**, 214666.
83 K. Zhang and R. Zou, *Small*, 2021, **17**, 2100129.
84 Z. Chen, X. Duan, W. Wei, S. Wang and B.-J. Ni, *J. Mater. Chem. A*, 2019, **7**, 14971–15005.
85 S. Singha Roy, R. K. Sharma, A. Karmakar, S. Nagappan, B. Pathak and S. Kundu, *Appl. Catal., B*, 2025, **371**, 125227.
86 D. A. Rakov, *Energy Adv.*, 2023, **2**, 235–251.
87 P. M. Bodhankar, P. B. Sarawade, P. Kumar, A. Vinu, A. P. Kulkarni, C. D. Lokhande and D. S. Dhawale, *Small*, 2022, **18**, 2107572.
88 A. Karmakar, K. Karthick, S. S. Sankar, S. Kumaravel, R. Madhu and S. Kundu, *J. Mater. Chem. A*, 2021, **9**, 1314–1352.
89 C. M. Ramos-Castillo, L. Álvarez-Contreras, N. Arjona and M. Guerra-Balcázar, *J. Phys. Chem. C*, 2024, **128**, 4161–4170.
90 M. Li, H. Li, X. Jiang, M. Jiang, X. Zhan, G. Fu, J.-M. Lee and Y. Tang, *J. Mater. Chem. A*, 2021, **9**, 2999–3006.
91 W. Jiang, A. Y. Faid, B. F. Gomes, I. Galkina, L. Xia, C. M. S. Lobo, M. Desmau, P. Borowski, H. Hartmann, A. Maljusch, A. Besmehn, C. Roth, S. Sunde, W. Lehnert and M. Shviro, *Adv. Funct. Mater.*, 2022, **32**, 2203520.
92 I. Galkina, A. Y. Faid, W. Jiang, F. Scheepers, P. Borowski, S. Sunde, M. Shviro, W. Lehnert and A. K. Mechler, *Small*, 2024, **20**, 2311047.
93 J. Du, Z. Li, L. Wang, Y. Ding, W. Ye, W. Yang and L. Sun, *Adv. Sci.*, 2025, **12**, 2416661.
94 Y. Shi, L. Song, Y. Liu, T. Wang, C. Li, J. Lai and L. Wang, *Adv. Energy Mater.*, 2024, **14**, 2402046.
95 J.-X. Wu, Y. Mao, Y. Zhou, Z. Wang, S. Wei, B. C. C. Cowie, A. T. Marshall, Z. Wang and G. I. N. Waterhouse, *Chem. Eng. J.*, 2025, **508**, 160753.
96 Y. S. Park, J.-Y. Jeong, M. J. Jang, C.-Y. Kwon, G. H. Kim, J. Jeong, J. Lee, J. Lee and S. M. Choi, *J. Energy Chem.*, 2022, **75**, 127–134.
97 C. Liang, P. Zou, A. Nairan, Y. Zhang, J. Liu, K. Liu, S. Hu, F. Kang, H. J. Fan and C. Yang, *Energy Environ. Sci.*, 2020, **13**, 86–95.
98 Z. Li, G. Lin, L. Wang, H. Lee, J. Du, T. Tang, G. Ding, R. Ren, W. Li, X. Cao, S. Ding, W. Ye, W. Yang and L. Sun, *Nat. Catal.*, 2024, **7**, 944–952.
99 H. Liu, R. Xie, Y. Luo, Z. Cui, Q. Yu, Z. Gao, Z. Zhang, F. Yang, X. Kang, S. Ge, S. Li, X. Gao, G. Chai, L. Liu and B. Liu, *Nat. Commun.*, 2022, **13**, 6382.
100 W. Li, Y. Ding, Y. Zhao, Z. Li, G. Lin, L. Wang and L. Sun, *Angew. Chem., Int. Ed.*, 2025, **64**, e202505924.
101 Y. Luo, Y. Yang, Y. Tian, Q. Wu, W.-F. Lin and M. Wen, *J. Mater. Chem. A*, 2025, **13**, 7136–7148.
102 Y. Song, M. Sun, S. Zhang, X. Zhang, P. Yi, J. Liu, B. Huang, M. Huang and L. Zhang, *Adv. Funct. Mater.*, 2023, **33**, 2214081.
103 Z. Cai, J. Liang, Z. Li, T. Yan, C. Yang, S. Sun, M. Yue, X. Liu, T. Xie, Y. Wang, T. Li, Y. Luo, D. Zheng, Q. Liu, J. Zhao, X. Sun and B. Tang, *Nat. Commun.*, 2024, **15**, 6624.
104 Y. Yin, S. Wang, B. Chen, A. Zhang, L. Wang, F. Bai, T. Wang, J. Zhang and Z. Che, *Small*, 2025, e08103.
105 A. Zaffora, B. Megna, B. Seminara, F. Di Franco and M. Santamaria, *Nanomaterials*, 2024, **14**, 407.
106 Y. Sun, G. Chen, F. El bachraoui, Y. Cui, G. Liu, F. Xiao, X. Qian, Z. Xu and M. Shao, *Small Methods*, 2025, **9**, 2500103.
107 F. Wu, F. Tian, M. Li, S. Geng, L. Qiu, L. He, L. Li, Z. Chen, Y. Yu, W. Yang and Y. Hou, *Angew. Chem., Int. Ed.*, 2025, **64**, e202413250.
108 P. Thangavel, G. Kim and K. S. Kim, *J. Mater. Chem. A*, 2021, **9**, 14043–14051.
109 M.-J. Zhao, E.-M. Li, N. Deng, Y. Hu, C.-X. Li, B. Li, F. Li, Z.-G. Guo and J.-B. He, *Renewable Energy*, 2022, **191**, 370–379.
110 M. Fang, W. Gao, G. Dong, Z. Xia, S. Yip, Y. Qin, Y. Qu and J. C. Ho, *Nano Energy*, 2016, **27**, 247–254.
111 X. Wang, Z. Jiang, Y. Ma, X. Su, X. Zhao, A. Zhu and Q. Zhang, *J. Power Sources*, 2024, **591**, 233819.
112 K.-Y. Yoon, K.-B. Lee, J. Jeong, M.-J. Kwak, D. Kim, H. Y. Roh, J.-H. Lee, S. M. Choi, H. Lee and J. Yang, *ACS Catal.*, 2024, **14**, 4453–4462.
113 A. Carbone, S. C. Zignani, I. Gatto, S. Trocino and A. S. Aricò, *Int. J. Hydrogen Energy*, 2020, **45**, 9285–9292.
114 C. Busacca, S. C. Zignani, A. Di Blasi, O. Di Blasi, M. Lo Faro, V. Antonucci and A. S. Aricò, *Int. J. Hydrogen Energy*, 2019, **44**, 20987–20996.
115 M. J. Jang, J. Yang, J. Lee, Y. S. Park, J. Jeong, S. M. Park, J.-Y. Jeong, Y. Yin, M.-H. Seo, S. M. Choi and K. H. Lee, *J. Mater. Chem. A*, 2020, **8**, 4290–4299.
116 X. Cui, Y. Ding, T. Tang, L. Wang, F. Zhang, P. Li, L. Sun and B. Zhang, *ACS Appl. Mater. Interfaces*, 2025, **17**, 29659–29668.
117 G. Lin, A. Dong, Z. Li, W. Li, X. Cao, Y. Zhao, L. Wang and L. Sun, *Adv. Mater.*, 2025, **37**, 2507525.
118 Y. S. Park, J. H. Lee, M. J. Jang, J. Jeong, S. M. Park, W.-S. Choi, Y. Kim, J. Yang and S. M. Choi, *Int. J. Hydrogen Energy*, 2020, **45**, 36–45.
119 K. C. Devarayapalli, J. Lee, S. Kang, S. Moon, S. V. P. Vattikuti, J. Lee and K. Lee, *J. Power Sources*, 2022, **527**, 231151.

120 Y. Kumar, S. Barik, N. S. Samudre, G. P. Kharabe, I. Chauhan, N. Manna, S. Bhat and S. Kurungot, *Adv. Sustainable Syst.*, 2025, **9**, 2400957.
121 H. Zhang, A. W. Maijenburg, X. Li, S. L. Schweizer and R. B. Wehrspohn, *Adv. Funct. Mater.*, 2020, **30**, 2003261.
122 J. Su, J. Zhou, L. Wang, C. Liu and Y. Chen, *Sci. Bull.*, 2017, **62**, 633–644.
123 K. Guo, M. Kunimoto and T. Homma, *J. Mater. Chem. A*, 2025, **13**, 7313–7323.
124 T. Kim, K.-R. Yeo, H. Kim, J. Lee and S.-K. Kim, *Int. J. Energy Res.*, 2025, 6685212.
125 T. Zhao, S. Wang, C. Jia, C. Rong, Z. Su, K. Dastafkan, Q. Zhang and C. Zhao, *Small*, 2023, **19**, 2208076.
126 W. Guo, J. Kim, H. Kim and S. H. Ahn, *Int. J. Hydrogen Energy*, 2021, **46**, 19789–19801.
127 A. Meena, P. Thangavel, D. S. Jeong, A. N. Singh, A. Jana, H. Im, D. A. Nguyen and K. S. Kim, *Appl. Catal., B*, 2022, **306**, 121127.
128 K. Singh and K. Selvaraj, *J. Colloid Interface Sci.*, 2024, **664**, 389–399.
129 F.-L. Wang, N. Xu, C.-J. Yu, J.-Y. Xie, B. Dong, X.-Y. Zhang, Y.-W. Dong, Y.-L. Zhou and Y.-M. Chai, *Appl. Catal., B*, 2023, **330**, 122633.
130 S. Kang, K. Ham and J. Lee, *Electrochim. Acta*, 2020, **353**, 136521.
131 C. Lee, Y. H. Yun, S. Kim, G. Doo, S. Lee, H. Park, Y. Park, J. Shin, H. Cho, S. Kim, E. Cho, C. Jung and M. Kim, *Small*, 2025, **21**, 2405468.
132 K. Wang, Y. Wang, Y. Chen, G. Deng, Y. Zhou and C. Xu, *Int. J. Hydrogen Energy*, 2025, **109**, 1108–1113.
133 B. Chen, F. Bai, Y. Feng, S. Wang, X. Cao, W. Li, L. Wang, X. Fu, L. Jin, J. Zhang, Y. Yin and M. D. Guiver, *J. Mater. Chem. A*, 2025, **13**, 9174–9183.
134 Q. Xu, S. Z. Oener, G. Lindquist, H. Jiang, C. Li and S. W. Boettcher, *ACS Energy Lett.*, 2021, **6**, 2238–2239.
135 S. S. Jeon, Y. Choi, J. W. Lee, R. Haaring, W. Lee, H. Jeon, J. Nam, E. Lee, S. Lee, M. Kim, Y. S. Jung, Y. Jung, Y. J. Hwang and H. Lee, *Adv. Energy Mater.*, 2025, **15**, 250180.
136 X. Lin, X. Li, L. Shi, F. Ye, F. Liu and D. Liu, *Small*, 2024, **20**, 2308517.
137 J. Zhou, S. Qiu, X. Hou, T. Ni, C. Zhang, S. Dai, X. Wang, G. Wang, H. Jiang and M. Huang, *Angew. Chem.*, 2025, **137**, e202503787.
138 Y. C. Lei, J. Zhou, W. Zhou, Y. Wang, M. Zhang, A. Zhang and L. Wang, *Chem. Commun.*, 2024, **60**, 11000–11016.
139 C. Hu, Y. Hu, B. Zhang, H. Zhang, X. Bao, J. Zhang and P. Yuan, *Electrochem. Energy Rev.*, 2024, **7**, 19.
140 W. Shen, Y. Ye, Q. Xia and P. Xi, *EES Catal.*, 2025, **3**, 10–31.
141 S. Singha Roy, S. Nagappan, A. K. Satheesan, A. Karmakar and S. Kundu, *J. Phys. Chem. C*, 2024, **128**, 13634–13650.
142 S. Park, J. H. Jun, M. Park, J. Jeong, J.-H. Jo, S. Jeon, J. Yang, S. M. Choi, W. Jo and J.-H. Lee, *Energy Fuels*, 2024, **38**, 4451–4463.
143 Y. S. Park, G. H. Choi, J. Jung, C.-H. Ahn, S. S. Hwang, M. G. Nam, P. J. Yoo and A. S. Lee, *ACS Catal.*, 2024, **14**, 9969–9984.
144 P. Thangavel, M. Ha, S. Kumaraguru, A. Meena, A. N. Singh, A. M. Harzandi and K. S. Kim, *Energy Environ. Sci.*, 2020, **13**, 3447–3458.
145 K. W. Ahmed, S. Habibpour, Z. Chen and M. Fowler, *J. Energy Storage*, 2024, **79**, 110149.
146 L. Osmieri, Y. He, H. T. Chung, G. McCool, B. Zulevi, D. A. Cullen and P. Zelenay, *J. Power Sources*, 2023, **556**, 232484.
147 A. Y. Faid, A. O. Barnett, F. Seland and S. Sunde, *Int. J. Hydrogen Energy*, 2022, **47**, 23483–23497.
148 U. Y. Lee, D. I. Jeong, J. S. Ha, J. H. Lee, H. Choi, J. H. Yoo, H. G. Choi, H. Y. Kim, B. K. Kang, Y. S. Park and D. H. Yoon, *Adv. Compos. Hybrid Mater.*, 2025, **8**, 140.
149 A. Meena, P. Thangavel, A. S. Nissimagoudar, A. Narayan Singh, A. Jana, D. Sol Jeong, H. Im and K. S. Kim, *Chem. Eng. J.*, 2022, **430**, 132623.
150 T. Jiang, X. Jiang, C. Jiang, J. Wang, Y. Danlos, T. Liu, C. Deng, C. Chen, H. Liao and V. Kyriakou, *Adv. Energy Mater.*, 2025, **15**, 2501634.
151 R. Balu, G. Devendrapandi, L. Gnanasekaran, P. C. Karthika, O. H. Abd-Elkader, W. K. Kim, V. R. Minnam Reddy, M. Kapoor, S. Singh and M. Lavanya, *Int. J. Hydrogen Energy*, 2024, **90**, 1378–1389.
152 Y. Yoon, S. Choi, J. Park, H. Baek, J. Jeon and T. Lim, *J. Am. Ceram. Soc.*, 2025, **108**, e20653.
153 Y. Kumar, S. Barik, N. S. Samudre, G. P. Kharabe, I. Chauhan, N. Manna, S. Bhat and S. Kurungot, *Adv. Sustainable Syst.*, 2025, **9**, 2400957.
154 G. Sriram, K. Dhanabalan, K. V. Ajeya, K. Aruchamy, Y. C. Ching, T. H. Oh, H.-Y. Jung and M. Kurkuri, *J. Mater. Chem. A*, 2023, **11**, 20886–21008.
155 L. J. Titheridge and A. T. Marshall, *ACS Energy Lett.*, 2024, **9**, 1288–1294.
156 C. Santoro, A. Lavacchi, P. Mustarelli, V. Di Noto, L. Elbaz, D. R. Dekel and F. Jaouen, *ChemSusChem*, 2022, **15**, e202200027.

